MODELING CARBON DIFFUSION AND ITS IMPACT ON BORON DIFFUSION IN SILICON AND SILICON GERMANIUM

MODELING CARBON DIFFUSION AND ITS IMPACT ON BORON DIFFUSION IN SILICON AND SILICON GERMANIUM

By
Samer Samir Rizkalla Rizk
B.Sc.

A Thesis
Submitted to the School of Graduate Studies in
Partial Fulfillment of the Requirements
for the Degree of
Masters of Applied Science

McMaster University
Hamilton, Ontario, Canada

MASTERS OF APPLIED SCIENCE (2005) McMASTER UNIVERSITY
(Electrical Engineering) Hamilton, Ontario, Canada

TITLE: Modeling Carbon Diffusion and its Impact on Boron Diffusion in Silicon and Silicon Germanium

AUTHOR: Samer Samir Rizkalla Rizk, B.Sc. (Ain Shams University, Cairo, Egypt)

SUPERVISOR: Dr. Yaser M. Haddara

NUMBER OF PAGES: xiii, 93

ABSTRACT

The integration of silicon germanium (SiGe) in the base of heterojunction bipolar transistors (HBTs) has recently put the alloy into prominence to produce fast-switching transistors. However, the thin highly doped SiGe base makes the transistor susceptible to base dopant outdiffusion during device processing, which results in device performance degradation. Adding carbon to the base was shown to significantly suppress boron outdiffusion and help retain the narrow as-grown profile. Dopant behavior in the presence of various species needs to be well understood and modeled for two reasons: (1) to have accurate and predictive process simulators; and (2) to obtain insight into process development.

Modeling carbon diffusion and its role in suppressing boron diffusion in silicon and SiGe has been studied by several groups. While boron diffusion is well-established, different modeling regimes have been developed for carbon diffusion. Each of the existing studies has focused on subsets of the available experimental data. We present a consistent and complete model that accounts for carbon and boron diffusion in silicon and SiGe, under equilibrium and non-equilibrium conditions. In our regime, carbon diffusion is modeled according to the kick-out and Frank-Turnbull mechanisms for diffusion; in addition, we incorporate the carbon clustering phenomenon. To completely model boron diffusion, we account for the boron-interstitial clustering (BICs) effect and the {311} defects that are associated with boron transient enhanced diffusion (TED). In the developed model we make use of the well-established literature data for carbon diffusion, as well as boron diffusion and Si self-diffusion. The model was verified by simulating experiments that involve boron and/or carbon diffusion in silicon and SiGe and cover the complete temperature range of 750 - 1070 °C. The test structures include published experiments in addition to recent experimental results obtained through collaboration, and feature diffusion in inert and oxidizing ambients, under rapid thermal annealing (RTA) conditions, as well as in the presence of implant damage. We also investigated the validation of the model without the inclusion of either the clustering or the Frank-Turnbull reactions.

ACKNOWLEDGMENTS

First and foremost, I thank God for all and everything.

"I like a teacher who gives you something to take home to think about besides homework" ~ Lilly Tomlin. I would like to express my appreciation to Dr. Yaser Haddara for the supervisor and great friend he is. He was and will always be a source of support and advice. During the course of this Master's degree, Dr. Yaser has created a friendly environment in our research group that made this experience a pleasant and unforgettable one. Thank you sir for being a great example.

I would also like to thank my fellow graduate students who have taken me as a friend. I am deeply honored and fortunate to know you.

Last but not least, I am deeply grateful to my parents Samir and Effat, who have made the past two years a delightful period of my life through their continuous love and support. To my brother George and sister Mariana, love you guys so much. I thank God for you all everyday.

TABLE OF CONTENTS

LIST OF FIGURES

LIST OF TABLES

LIST OF COMMON SYMBOLS

I	Silicon self-interstitial
V	Silicon vacancy
A_s	General dopant atom occupying a substitutional site
A_i	General dopant atom occupying an interstitial site
AI	Dopant-interstitialcy pair
AV	Dopant-vacancy pair
B	Boron
C	Carbon
C_s	Substitutional carbon atom
C_i	Interstitial carbon atom
C_iC_s, Cl	Interstitial-substitutional carbon pair (Cluster)
C_X	Concentration of X (I, V, B, C_i, C_s, Cl, etc.)
C_X^*, C_X^{eq}	Equilibrium concentration of X
J_X	Flux of X
D_X	Diffusivity coefficient of X
D_X^*, D_X^{eq}	Equilibrium diffusivity of X
D_X^{eff}	Effective diffusivity of X
f_I	Fractional interstitial component of diffusion

n_i	Intrinsic carrier concentration
p	Hole concentration
n	Electron concentration
KO	Kick-out reaction
FT	Frank-Turnbull reaction
Cl	Clustering reaction
$k_{f,\mathrm{Reaction}}$	Forward reaction rate
$k_{r,\mathrm{Reaction}}$	Reverse reaction rate

Chapter 1

INTRODUCTION

Research in semiconductor device physics and technology has been sustained for the last decades and has continually improved the state of the art. To date, the semiconductor industry has been successful in exponentially shrinking the minimum feature size thus increasing the number of transistors on a chip, increasing device bandwidth, and increasing circuit complexity and functionality, as predicted by Moore's Law [1]. Several innovations have allowed this continual shrinking from one technology generation to the next. The incorporation of the silicon germanium (SiGe) alloy is one such development. This has been explored since the early nineties, and has seen increasing use in mainstream Si-based products over the last few years.

Semiconductor alloys provide device engineering with a wide range of energy gaps and mobilities, so that materials are available with properties that match specific applications. They demonstrate superior properties beyond the physical limits of the electronic properties of silicon, which is the most popular material used today to make electronic devices. Gallium arsenide (GaAs) and indium phosphide (InP) are compound semiconductors that have found application in niche markets due to their superior performance. By contrast, SiGe is attractive because of its compatibility with conventional Si technology.

Being a low cost microelectronic technology for integrated circuits, silicon technology has dominated the semiconductor industry for over 30 years [2], and the processing of silicon has become a mature technology. SiGe can be integrated with traditional Si technology allowing the introduction of fast switching heterojunction bipolar transistors (HBTs) with SiGe forming the base material in a BiCMOS process, or being incorporated in MOSFETs with SiGe forming the channel to enable device manufacturers to overcome challenges to the further scaling of CMOS.

As device dimensions continue to shrink controlling the profiles of dopants incorporated in the host material becomes critical. Significant degradation of device performance is known to occur due to the diffusion of dopants over short distances. Thus, the fabrication of microelectronic devices, and consequently their performances are based on tightly controlling the dopants' profiles in spatially restricted host regions. The introduction of the SiGe alloy in local device regions further complicates the problem because it adds the need to control the diffusion of Ge atoms in the host alloy as well as dopant atoms in the alloy. As well, the behavior of dopants must now be understood and controlled in a background of varying composition. Modeling dopant diffusion is therefore fundamental in order to have accurate and predictive process simulators, and physics-based models for dopant diffusion are required to provide process engineers with insight into process development, not just as a tool to empirically model a process flow after the fact.

1.1 Motivation

The advent of SiGe HBTs represents the first practical bandgap-engineering of Si-based transistors. When Ge is introduced into Si, the SiGe alloy features a bandgap smaller than that of Si, making Si suitable for bandgap engineering. This is due to the fact that Ge has a larger lattice constant than Si, and consequently a smaller bangap (0.66 eV versus 1.12 eV). Furthermore, the lattice constant mismatch produces compressive strain in SiGe alloys, which results in an additional bandgap reduction. The net bandgap shrinkage in SiGe alloys is approximately 7.5 meV per 1 % of Ge [3]. This "band offset" occurs primarily in the valence band of the SiGe base, making it conductive for use in *npn* transistors, as illustrated in Figure 1.

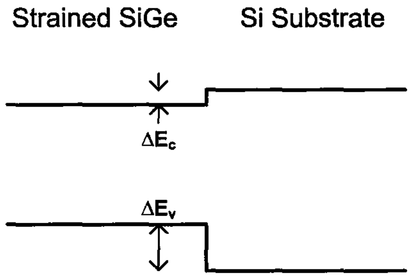

Figure 1: Schematic band alignments of strained SiGe grown on a Si substrate [4].

In addition, the introduced compressive strain lifts the conduction and valence band degeneracies at the band extremes, which results in reducing the density of states, hence improving the carrier mobilities with respect to silicon. Moreover, to achieve high frequency performance, the base region of a transistor must be thin, which makes SiGe a natural candidate for use in the base region, since practical SiGe layers must be very thin to ensure stable, defect-free layers. In SiGe *npn* HBTs, the bases can be heavily doped to reduce the base resistance, and hence increase the maximum oscillation frequency $f_{\max}$. Heavily doped bases also result in reducing the minimum noise figure [5],[6],[7]. In conclusion, SiGe HBT technology is far superior to Si bipolar transistors; they have higher dc-current gain β, higher maximum frequency $f_{\max}$, higher cut-off frequency f_T, lower gate delays, and better broad-band noise characteristics [3]. Table I presents a relative performance comparison of various device technologies for RFICs including the SiGe HBT and Si BJT.

Table I: Relative performance comparisons of various device technologies (Excellent: ++; Very good: +; Good: 0; Fair: –; Poor: – –) [4].

Performance Metric	SiGe HBT	Si BJT	Si CMOS	III-V MESFET	III-V HBT	III-V HEMT
Frequency Response	+	0	0	+	++	++
1/f and phase noise	++	+	–	– –	0	– –
Broadband Noise	+	0	0	+	+	++
Linearity	+	+	+	++	+	++
Output conductance	++	+	–	–	++	–
Tranconductance/area	++	++	– –	–	++	–
Power dissipation	++	+	–	–	+	0
CMOS integration	++	++	N/A	– –	– –	– –
IC cost	0	0	+	–	–	– –

However, the key feature of SiGe HBTs, the thin heavily doped base, makes it highly susceptible to base dopant (boron) outdiffusion during device processing. Diffusion of base dopant in SiGe HBTs into the neighboring silicon emitter and collector results in significant degradation in device performance [8]. For example, while typical base doping in HBTs is in the range of 10^{19} cm^{-3}, the emitter doping level is kept below 5×10^{18} cm^{-3} to avoid tunneling [8]. Any base dopant outdiffusion will therefore not be compensated by the n^+ emitter dopant. Hence, outdiffusion will lead to the broadening of the base profile pushing the *pn* base-emitter junction into the silicon. This introduces parasitic electron barriers in the conduction band that lead to reducing the collector current which is exponentially dependent on the barrier height. Only a few nanometers shift may cause severe device degradation, decreasing the gain, Early voltage and speed [8],[9]. Base dopant outdiffusion is typically caused by transient enhanced diffusion (TED) due to arsenic emitter and/or extrinsic boron implantation and anneal, which are typical steps in a BiCMOS process flow. Attempting to maintain low thermal budgets and eliminating implantation and annealing to minimize boron outdiffusion would impose stringent limits on the integration of SiGe into base line silicon technology.

It is therefore a key issue to SiGe HBT technology to retain the narrow high-concentration as-grown base profile of the SiGe base. The optimization of the Ge profile in SiGe HBTs is not sufficient to suppress boron outdiffusion. Undoped SiGe spacer layers grown on either side of the doped SiGe base have been studied to accommodate for the *pn* junction shift into the silicon regions [10]. However, the "critical thickness" of the SiGe strained films poses a limitation on the thickness of these undoped spacer layers. Recently, it has been shown that the incorporation of substitutional carbon into Si/SiGe has the effect of highly suppressing boron diffusion [11],[12],[13]. Original research of adding carbon to compressive-strained SiGe was motivated by carbon's ability to reduce strain and enhance thermal stability [14]. Suppression of boron diffusion in the base of

$Si_{1-x-y}Ge_xC_y$ HBTs via uniform and localized low carbon concentrations (~10^{20} cm^{-3}) was shown to significantly enhance HBT technology performance [9],[15],[16].

The focus of this work is modeling the suppression of boron diffusion in Si/SiGe due to the incorporation of localized substitutional carbon concentrations. Several studies exist that model the suppression of boron diffusion due to carbon. Each of these studies has focused on a subset of the available experimental data and sample structures. Several studies have considered the ability of carbon to reduce enhanced boron diffusion due to ion implantation or oxidation. Different approaches for incorporating the effect of carbon have been adopted. In this work, we present a consistent and complete model that accounts for carbon diffusion and its effect on boron diffusion. In the developed model we make use of the well-established published data for carbon diffusion, as well as boron diffusion and silicon self-diffusion. The model successfully accounts for boron and carbon behaviors in a wide range of sample structures and experimental conditions over the complete temperature range of 750 - 1070 °C in inert and oxidizing ambients, as well as in the presence of implant damage. The samples presented include a variety of experimental structures, in addition to recent experimental results obtained through collaboration. The model successfully accounts for the boron diffusion reduction under rapid thermal annealing (RTA), as used in typical BiCMOS technologies (1000-1100 °C) for dopant activation. It also accounts for the suppression of boron transient enhanced diffusion (TED) and oxidation enhanced diffusion (OED).

1.2 Methodology

This section presents the methodology and procedural flow typically followed to study impurity behavior in semiconductor materials, with focus on samples relevant to this research work. The study of dopant diffusion in a sample structure includes experimental and simulation work.

Dopants are normally introduced into test structures during wafer growth. Growth techniques include CVD (chemical vapor deposition) and MBE (molecular beam epitaxy). Ion implantation, which is a typical BiCMOS process step, is known to result in the creation of point defect (primarily interstitial) damage in the implant region. To observe the effect of ion implantation on dopant diffusion in some samples, the samples undergo an implantation step. Test structures with grown-in dopants, implanted or unimplanted, are then subjected to annealing in either inert or oxidizing ambients at different temperatures. Conventional annealing methods include furnace annealing and rapid thermal annealing. Dopant concentration profiles in unannealed and annealed samples are then measured for comparison between the initial and final profiles, respectively. Typical techniques for measuring concentration profiles include SIMS (secondary ion mass spectrometry), TOF-SIMS (time-of-flight secondary ion mass spectrometry), and RBS (Rutherford backscattering spectrometry). SIMS is the technique used for most samples studied in this work, and will be described later.

To simulate the experimental results, we performed 1D simulations using the FLOOPS-ISE software [17], which is a reliable and widely-used process simulator. FLOOPS-ISE features advanced physical models for semiconductor fabrication processes, as discussed in Chapter 2. In addition, it provides flexibility to define new materials and models (further details are discussed hereafter). For the samples presented in this work, and as in typical process simulators, sample structures are defined by specifying wafer dimensions, materials properties, and initial grown-in dopant profiles. Annealing temperatures and ambients are also specified. Plots of initial and final concentration profiles are then viewed for comparison.

In this work, we simulate several test structures described in the literature that contain boron and carbon in Si, SiGe or both. In addition, we simulate recent experiments involving boron diffusion in a SiGeC region, which were obtained through collaboration with a group in IMEC (Interuniversity MicroElectronics Center) and Katholieke Universiteit Leuven in Belgium [18]. At an earlier stage of our research work we annealed a set of samples containing boron in SiGeC layers, and attempted to measure C, B, and Ge profiles using TOF-SIMS, but were not successful in characterizing the concentration profiles of C and B.

1.2.1 Secondary Ion Mass Spectrometry (SIMS)

Secondary ion mass spectrometry or SIMS is a widely-used technique to measure the concentration of trace elements in solid materials, particularly thin film semiconductors [19]. It can be practically used to trace elements at very low concentrations (ppb-range). As shown in Figure 2, it is based on bombarding a sample surface with a high energy ion beam, the primary beam, and then using mass spectrometry to count the yield of one or more species of secondary, i.e. sputtered, ions.

The sputtering, which is the interaction of the primary ion beam with the sample surface, results in mixing the upper layers of the sample, which leads to the amorphization of the surface. While the primary ions are implanted into the sample, the secondary beam is emitted from the sample surface. The secondary beam is made up of electrically neutral as well as charged species. With the help of an electric field between the sample and the extraction lens, charged species of one polarity are extracted to the mass spectrometer. In the mass spectrometer, ions are sorted by mass (and energy) and then counted using an ion detector. The composition of the sputtered area is then analyzed by comparing the yields of different secondary ion species. Since the sample is slowly sputtered, SIMS is capable of measuring depth profiles.

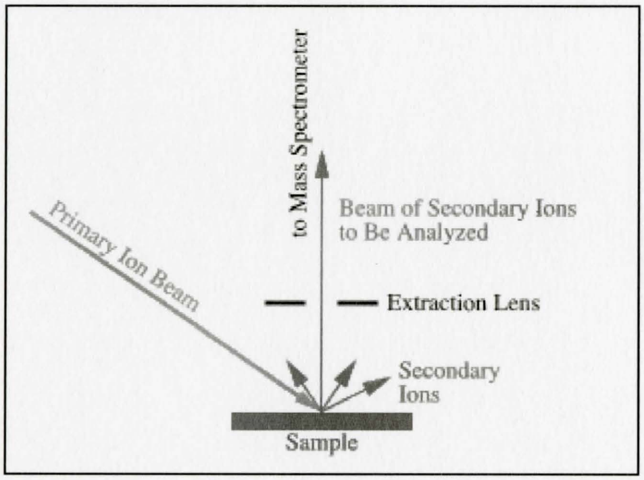

Figure 2: SIMS measurement technique [20].

Apart from noble gases that do not ionize easily, SIMS can be used to trace all elements of the periodic table.

1.2.2 FLOOPS-ISE

We used the process simulator FLOOPS-ISE in our work [17]. FLOOPS-ISE offers programmability to add new materials and define new diffusion models. It uses the Alagator scripting language allowing users to develop their own models for diffusion, in addition to the incorporated physical models.

In the complete model that we developed, discussed in Chapter 4, some parts were implemented using the models originally incorporated within FLOOPS-ISE such as for boron diffusion, whereas for carbon diffusion we implemented our model using Alagator to define a system of partial differential equations that describes carbon diffusion.

1.3 Thesis Organization

There are seven chapters in this thesis. The physical phenomena associated with the diffusion of boron and carbon in Si and SiGe are presented in Chapter 2. We start by discussing the general dopant diffusion mechanisms, which are categorized as either simple or complex diffusion mechanisms. Followed by this, we elaborate on the specific mechanisms for boron and carbon diffusion, and the effects associated with boron enhanced diffusion and the carbon clustering phenomenon. The impact of substitutional carbon on boron diffusion in Si and SiGe is then explained.

In Chapter 3, a literature review of existing studies on modeling carbon diffusion and its effect on boron diffusion in Si and SiGe is presented. We start by providing an analysis of the involved diffusion parameters. Next, we present the various existing approaches for modeling the carbon behavior.

In Chapter 4, we present a consistent and complete model for C diffusion and its impact on B diffusion under equilibrium and non-equilibrium conditions. In Chapter 5, comparison between experiment and simulation obtained using our model is verified over a wide range of samples. Chapter 6 considers the validation of the model over the samples without the inclusion of all the model reactions. And finally, the work is concluded in Chapter 7, and future directions for research are proposed.

Chapter 2

DIFFUSION IN Si/SiGe

Diffusion in its simplest form can be described as the motion of atoms down a concentration gradient. In the simplest case, diffusion may be described in one dimension using Fick's first and second laws:

$$J = -D\frac{\partial C}{\partial x}, \tag{1}$$

$$\frac{\partial C}{\partial t} = -\frac{\partial}{\partial x}J = D\frac{\partial^2 C}{\partial x^2}, \tag{2}$$

where C is the diffusant concentration and J is the diffusion flux. The diffusivity parameter D hides the physics of the diffusion process, and is in general a function of temperature and concentration. Understanding the atomistic mechanisms by which diffusants behave in the host material and modeling the diffusion process entails the derivation of a form for D that completely describes its dependence on process conditions and other material properties.

2.1 Diffusion Mechanisms

2.1.1 Simple Diffusion Mechanisms

The simplest diffusion mechanisms, as schematically described in Figure 3, are the ring, interstitial and vacancy mechanisms [21]. The ring mechanism, Figure 3(a), is the simplest method and does not involve interaction with point defects. In this mechanism, diffusion occurs through direct exchange of two particles. In a crystalline material, the tightly packed structure would make such exchange highly unlikely because neighboring atoms must be compressed before they can squeeze past each other and exchange positions. Therefore, a more likely scenario for the ring diffusion mechanism takes place via a cyclical exchange involving three or more particles. The ring mechanism has not been experimentally demonstrated and is therefore not generally used to explain real diffusion data.

The interstitial diffusion mechanism, Figure 3(b), is the dominant one for most interstitial solutes (e.g. Cu, Li in Si) [21]. In this case, the diffusant atom jumps from one interstitial position to a neighboring one. This is energetically plausible for small interstitial atoms but less likely for large ones.

The vacancy mechanism, Figure 3(c), is accepted as the dominant mechanism for diffusion of substitutional impurities in metals [21]. In this mechanism, a substitutional atom jumps from its lattice site onto an adjacent vacancy. The diffusivity is therefore dependent on the probability of finding a vacancy on an adjacent site, which in turn makes it proportional to the mole fraction of vacancies in the lattice. The resultant is a flux of vacancies equal and opposite to the flux of the diffusing species.

While the above simple models explain the diffusion behavior in many applications, they do not suffice to account for the diffusion of common dopants in semiconductors involving interaction with intrinsic point defects. Additionally, under conditions of point defect non-equilibrium, the observed diffusion could in fact only be explained in terms of more complex diffusion mechanisms, which are briefly described here.

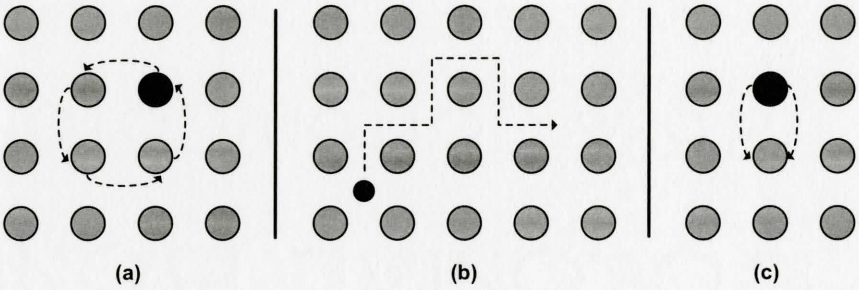

Figure 3: Direct interstitial (a), vacancy (b), and ring (c) diffusion mechanisms in a diamond lattice [22].

2.1.2 Complex Diffusion Mechanisms

A common notion used in modeling advanced diffusion mechanisms is that a quasi-chemical equilibrium is maintained between two species involving the impurity: (1) the impurity as an immobile substitutional atom, and (2) a fast-diffusing species that involves the impurity. Modeling of impurity diffusion can be achieved by writing and solving simultaneously the continuity equations for all species involved in maintaining the equilibrium between the mobile and immobile impurity species. The resultant effective diffusivity depends on $\partial C_{\text{mobile}} / \partial C_{\text{totoal}}$, where C_{mobile}, and C_{total} represent the mobile and total impurity concentrations, respectively [21].

In a crystalline material, a single atom residing on a lattice site is known as a "substitutional defect", whereas when two atoms share a single lattice site it is known as an "interstitialcy defect". In silicon, dopants dissolve in the lattice almost exclusively on substitutional sites. We will use the symbol A_s to denote a dopant atom occupying a substitutional site surrounded only by silicon atoms. When a vacancy, V, resides next to a substitutional dopant atom and is bound to it in some fashion this is referred to as a "dopant-vacancy pair", denoted AV. The symbol AI is used to denote both an interstitialcy defect and a dopant-interstitial pair, where I is a silicon interstitial. If a dopant atom itself is occupying an interstitial position it is known as an interstitial dopant, A_i. Diffusion occurs through the migration of the AV, AI, or A_i defects. The reactions governing defect formation and dissolution are given by:

$$A_s + V \Leftrightarrow AV, \tag{3}$$

$$A_s + I \Leftrightarrow AI, \tag{4}$$

$$A_s + I \Leftrightarrow A_i, \tag{5}$$

$$A_i + V \Leftrightarrow A. \tag{6}$$

Equation (3) describes the formation of dopant-vacancy pairs and is illustrated in Figure 4. When the dopant atom binds to a host vacancy through Coulombic attraction, the dopant-vacancy pair becomes the primary diffusing species. This mechanism yields a higher diffusivity than the pure vacancy (substitutional) mechanism due to the Coulombic binding force, which increases the probability of finding a vacancy nearby. For long-range migration of the dopant to take place, the dopant-vacancy pair must dissolve some distance away from the dopant atom's starting position so that the vacancy may bind to another atom along a different path.

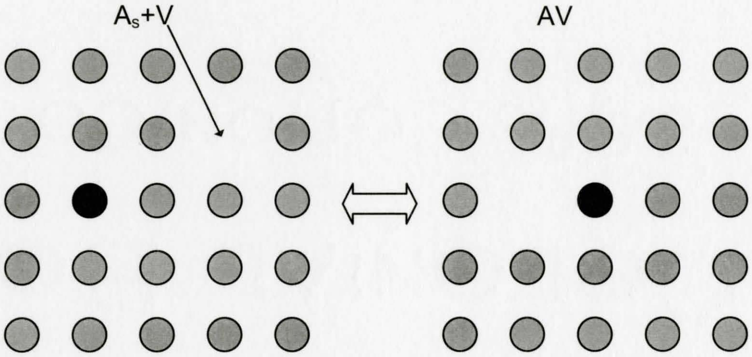

Figure 4: Dopant-vacancy pair diffusion mechanism [22].

Reaction (4) describes dopant diffusion by an interstitial-pair mechanism (sometimes called the substitutional-interstitialcy mechanism) while Eq. (5) depicts the kick-out mechanism, which is one of a class of models known as substitutional-interstitial models. Both mechanisms are *mathematically* equivalent. Equations (4) and (5) are known as "kick-out" reactions. The interstitial-pair mechanism is illustrated in Figure 5(a). In this mechanism diffusion occurs via interstitialcy defects (two atoms sharing a single lattice site). Diffusion takes place when the dopant jumps toward an adjacent lattice site, already occupied by a silicon atom, where it associates with the new silicon atom to form a new interstitialcy defect. In the kick-out mechanism of Eq. (5) diffusion occurs by interstitial defects, where a silicon interstitial diffuses through the interstices of the lattice until it reacts with a substitutional dopant atom, as shown in Figure 5(b). A kick-out reaction then takes place causing the dopant atom to be dislodged becoming a dopant interstitial. The dopant interstitial then diffuses through the lattice interstices until it returns to a substitutional position by dislodging a silicon atom in the reverse reaction.

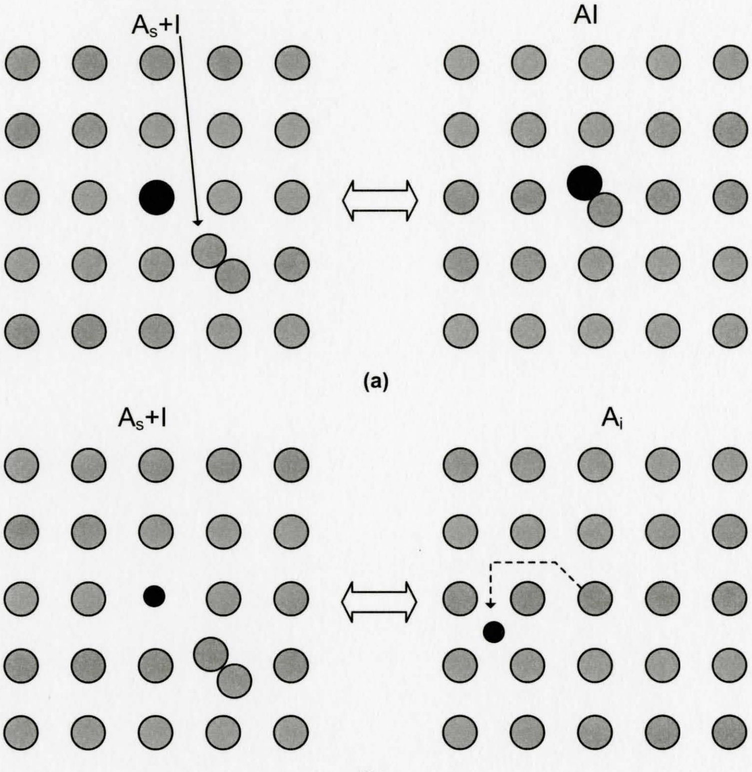

Figure 5: Interstitial-pair (a), and kick-out (b) diffusion mechanisms [22].

Finally, interstitial dopants may react with lattice vacancies to become substitutional atoms as shown in Figure 6; this reaction is described by Eq. (6), and is referred to as the dissociative reaction or the "Frank-Turnbull" [23]. The Frank-Turnbull mechanism is also a substitutional-interstitial diffusion mechanism.

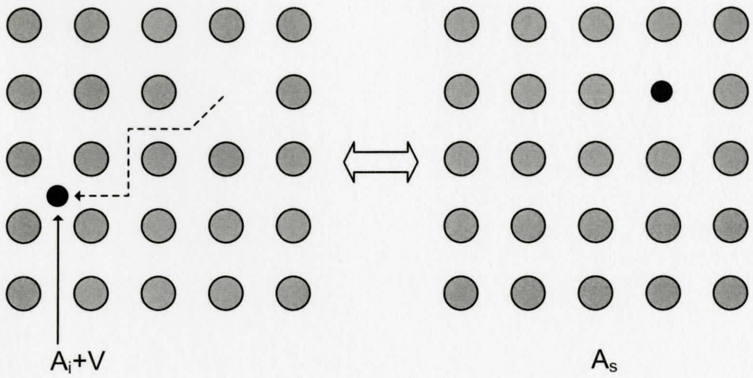

Figure 6: The Frank-Turnbull mechanism [22].

In each of the above models the dopant effective diffusivity depends on the ratio between the mobile and immobile species. This ratio depends on the number of defects available for the reaction, but it also involves charge carriers depending on the charge state of each of the species participating in the reaction. Hence the effective diffusivity is affected both by carrier concentrations and by point defect concentrations. The dependence on carrier concentration, or equivalently the Fermi level, adequately explains observed concentration-dependent diffusion when the dopant concentration is sufficiently high to make the semiconductor extrinsic at process temperatures in the absence of perturbations to point defect equilibrium, while the dependence on defect concentrations explains non-equilibrium diffusion behavior when point defect equilibrium is perturbed, e.g. due to damage or surface treatment that results in excess defects. Finally, it should be noted that an actual dopant may diffuse by a combination of interstitial and vacancy mediated mechanisms.

2.2 Non-equilibrium Dopant Diffusion by Perturbations in Point Defect Concentrations

As mentioned earlier, a change in point defect concentrations will cause non-equilibrium diffusion. For example, annealing pure Si in an oxidizing ambient is known to inject interstitials whereas annealing in a nitriding ambient is known to inject vacancies [24]. The diffusion of a given dopant species will be enhanced or retarded in each of these cases depending on what fraction of its diffusion occurs by interaction with each defect species. The steady-state dopant diffusivity under non-equilibrium conditions is determined relative to the diffusivity under equilibrium conditions in terms of super/under-saturation of interstitials and vacancies respectively:

$$\frac{D_A}{D_A^*} = f_I \frac{C_I}{C_I^*} + (1 - f_I)\frac{C_V}{C_V^*}, \tag{7}$$

where the subscripts I and V denote interstitial and vacancy respectively, the superscript * denotes equilibrium conditions, and f_I is the fractional interstitial component of diffusion.

Silicon interstitials and vacancies are annihilated through recombination, so that there is generally an undersaturation of one when there is a supersaturation of the other. This may be expressed in terms of the mass-action law, which relates the equilibrium concentrations to the actual concentrations when the recombination process is fast:

$$C_I C_V = C_I^* C_V^*. \tag{8}$$

2.3 Boron Diffusion in Si and Strained SiGe

As mentioned earlier dopant diffusion may take place through combined mechanisms. Hence, a dopant could diffuse through entirely one or both the substitutional-interstitial(cy) mechanism and the vacancy mediated mechanism, with varying interstitial contribution to the diffusion (f_I). Boron dissolves in silicon substitutionally and it is generally agreed that boron diffusion occurs almost entirely through an interstitial mediated motion (f_I~98%) [25], either as an interstitial or an interstitialcy. In either case, the reaction may be modeled by the following equation [26]:

$$B_s^i + Si_i^l + (j-l-i)p \Leftrightarrow B_i^j + Si_s, \qquad (9)$$

where i is the original charge on the dopant substitutional atom, l is the charge on the silicon interstitial, j is the charge on the mobile dopant species, and the silicon substitutional atom is assumed to be uncharged [26]. Since boron acts as an acceptor dopant in silicon with a -1*e charge, i=-1. In the vacancy mediated mechanism, the reaction between the substitutional boron atom and the silicon vacancy may be modeled by the following reaction [26]:

$$(B_s^i)_{\text{site A}} + (Si_v^l)_{\text{site B}} + (j+m-l-i)p \Leftrightarrow (B_s^j)_{\text{site B}} + (Si_v^m)_{\text{site A}}. \qquad (10)$$

where i and l are the original charges on the substitutional atom and silicon vacancy, respectively, while j and m are the new charges on the substitutional dopant and vacancy, respectively.

Taking this into account, noting the fact that substitutional boron is immobile and only the mobile defects contribute to boron diffusion, and taking into account the effect of carrier concentration, we may write the boron diffusivity in extrinsic Si as:

$$D_{B,\text{defect}} = D_{B,\text{defect}^0} + \frac{p}{n_i} D_{B,\text{defect}^+}, \tag{11}$$

where

$$\begin{aligned} D_{B,I} &= D_B^{\text{eq}} \times f_I = D_{B,I^0} + \frac{p}{n_i} D_{B,I^+}, \\ D_{B,V} &= D_B^{\text{eq}} \times (1 - f_I) = D_{B,V^0} + \frac{p}{n_i} D_{B,V^+}, \end{aligned} \tag{12}$$

where the superscript eq denotes equilibrium. The activation energies, as well as the ratios between the coefficients for interstitial and vacancy mediated dopant diffusion appear to be the same for a given dopant, with no theoretical explanation for this [26]. Given the above dual diffusion mechanism, a simple form for the total boron particle current can be given by [26]:

$$J_{B,\text{total}} = D_B^{\text{eq}} C_B \times \left(f_I \frac{C_I}{C_I^*} \nabla \ln\left((\frac{p}{n_i}) C_B \frac{C_I}{C_I^*} \right) + (1 - f_I) \frac{C_V}{C_V^*} \nabla \ln\left((\frac{p}{n_i}) C_B \frac{C_V}{C_V^*} \right) \right), \tag{13}$$

where C_B is the substitutional boron concentration.

As confirmed for the other group III and group V dopants, it is probable that boron diffuses via a vacancy mediated mechanism in pure germanium, which implies a changeover of dominant diffusion mechanism for boron diffusion in $Si_{1-x}Ge_x$ at some composition x [27]. The behavior of boron in SiGe with high germanium content is unclear [28]. However, for a germanium fraction below ~20% it has been reported that the diffusion mechanism for boron in SiGe is still primarily interstitial as is the case in pure Si [29],[30]. There is general agreement that boron diffusion in strained $Si_{1-x}Ge_x$ is retarded as the germanium content increases (for $x \leq 0.5$) [31],[32]. However, there is little agreement on the reason behind this diffusion retardation. Kuo *et al.* concluded that the diffusion reduction is attributed to the change in point defect concentration caused by the band-gap narrowing [31], whereas the analysis given by Moriya *et al.* suggests that the reduction in boron diffusivity in $Si_{1-x}Ge_x$ is predominantly a function of the germanium content and that the retardation is from Ge-B paring, rather than the strain [32].

In the following two sections we discuss phenomena that are of particular interest in modeling the boron diffusion process: (1) oxidation enhanced diffusion due to annealing in an oxidizing ambient, and (2) transient enhanced diffusion due to ion implantation.

2.3.1 Oxidation Enhanced Diffusion (OED)

As mentioned earlier, oxidation of pure silicon is known to inject interstitial defects. Since boron is primarily an interstitial diffuser this results in enhanced diffusion in Si and SiGe in a phenomenon known as oxidation enhanced diffusion (OED) [29],[30]. OED has been studied extensively in Si and SiGe; LeGoues *et al.* reported that boron OED is suppressed in silicon when oxidizing a silicon substrate capped with a thin $Si_{0.5}Ge_{0.5}$ layer [33]. In addition, suppressed boron OED in silicon co-implanted with boron and germanium has also been reported [34]. However, OED proceeds without reduction in a layer of $Si_{1-x}Ge_x$ ($x<0.3$) capped with a sufficiently thick silicon layer [30].

2.3.2 Transient Enhanced Diffusion (TED)

The "anomalous" phenomenon of transient enhanced diffusion (TED) occurs when crystalline silicon is ion-implanted and then subjected to thermal annealing. TED is caused by excess point defects in the region of implant damage. Intuitively, one would expect the damage to be primarily interstitial since the implant process *adds* material. These interstitials would dramatically enhance the diffusion of any dopant that diffuses, even in part, by an interstitial mediated mechanism. For boron, which is primarily an interstitial diffuser, the initial enhancement would be several orders of magnitude (corresponding to the excess interstitial population). However, as time progresses, excess interstitials would diffuse from the damage region into the bulk, where they would be annihilated through bulk recombination, and to the surface, where they would be annihilated through surface recombination. Given known values for interstitial and vacancy diffusivities, D_I and D_V, these processes would result in the equilibrium of interstitial and vacancy concentrations in a very short period of time, on the order of a few minutes. Contrary to this expectation, experimental data show that the transient diffusion enhancement lasts for a longer period of time, and is characterized by an exponential time decay with a large time constant, on the order of 2 hours at 750 °C as reported by Robertson *et al.* [35]. This would indicate that there is one or more mechanisms to store and release the excess interstitials. Eaglesham *et al.* suggested that

TED is caused by the emission of interstitials from {311} defects [36]. Later Zhang *et al.* reported that they observed TED in samples without the aforementioned {311} defects and they attributed the source of TED to submicroscopic clusters [37], that are now commonly referred to as boron interstitial clusters (BICs) [38]. Much experimental and theoretical work has been carried out to investigate the above mechanisms [39],[40],[41].

The {311} defects are interstitial agglomerates that are formed following implantation and during the initial stages of annealing, providing a mechanism that stores and releases excess interstitials. These are "rodlike" defects extending along the $\langle 110 \rangle$ directions located on the {311} habit planes as single monolayers of hexagonal silicon [36]. The excess interstitial concentration contained in the {311} defects is agreed to be approximately equal to the implantation dose [39]. The dissolution of the {311} defects and the subsequent number of interstitials released during annealing is correlated with the flux of interstitials driving TED and the length of the diffusion transient [36].

Clustering of boron atoms even at concentrations far below the dopant's equilibrium solubility in silicon is caused by ion-implantation. The formation of boron interstitial clusters (BICs) is proposed as a secondary buffer for the interstitial supersaturation associated with ion implantation [38]. The nucleation of immobile BICs occurs when excess interstitials drive substitutional boron into electrically inactive, metastable clusters of presumably two or more boron atoms during the early stages of TED [39]. A wide range of different size BICs can be formed; a general representation of the BICs defect family is given in the form $\mathrm{B}_{n\mathrm{B}}\mathrm{I}_{n\mathrm{I}}$ where n_B and n_I are the numbers of boron atoms and interstitials in the defect respectively. There is no precise agreement on how BICs are involved in TED [38]; however, the interstitials released from the dissolution of BICs during annealing contribute to the enhanced diffusion. This BICs formation is also known to be responsible for boron deactivation which persists even after TED is over; Stolk *et al.* have reported that immobile boron clusters remained at the initial level upon continued annealing in the temperature range of 550-720 °C, whereas at 790 °C the decay time was on the scale of ~10 hours [39].

Several studies exist that model the {311} defects [41],[42], and the BICs formation [13],[43]. Chapter 4 presents the models that we have implemented for the above effects.

2.4 Carbon Diffusion in Si and SiGe

Carbon is predominantly a substitutional solute in silicon that diffuses relatively fast in terms of the substitutional-interstitial exchange mechanism [44], with an interstitial diffusivity fraction close to one ($f_I \approx 1$) [45]. The mobile diffusing species (C_i) is interstitial-like and occurs as a minor fraction relative to the much more abundant but immobile substitutional configuration (C_s). The change-over between the interstitial and substitutional carbon occurs via the kick-out and dissociative mechanisms (Eqs. 4 and 5). The above carbon diffusion mechanism predicts that, as carbon diffuses out of a given region, an effective flux of interstitials arises *out of* that region and an effective flux of vacancies *into* it. At high carbon concentrations, greater than its solid solubility in silicon, the product of the C concentration (C_{C_s}) and the equilibrium carbon diffusivity

($D_{C_s}^{\mathrm{eff}}$) exceeds the corresponding transport parameters for the fluxes of self-interstitials and vacancies [13],[46]:

$$D_{C_s}^{\mathrm{eff}} C_{C_s} > D_I C_I^{\mathrm{eq}}, \qquad D_{C_s}^{\mathrm{eff}} C_{C_s} > D_V C_V^{\mathrm{eq}}. \tag{14}$$

Under these conditions, the outdiffusion of C from C-rich areas becomes limited by the corresponding fluxes of Si point defects, which results in an undersaturation of interstitials and a supersaturation of vacancies in those regions. The effective equilibrium carbon diffusivity is determined by the diffusivity of the only mobile C species C_i times it relative abundance at equilibrium and is given by [13],[47]:

$$D_{C_s}^{\mathrm{eff}} = D_{C_i} \frac{C_{C_i}^{\mathrm{eq}}}{C_{C_s}^{\mathrm{eq}}}, \tag{15}$$

where $C_{C_s}^{\mathrm{eq}}$ is the carbon solubility, $C_{C_i}^{\mathrm{eq}}$ is the interstitial carbon solubility, and D_{C_i} is the interstitial carbon diffusivity.

Carbon diffusion in silicon is further complicated by carbon clustering, which we discuss next.

2.4.1 Carbon Clustering

Recent interest in incorporating carbon in silicon arises primarily from its role in retarding boron diffusion, particularly in HBT structures as briefly discussed in Chapter 1. For this type of application, carbon is incorporated during growth by chemical vapor deposition (CVD) or molecular beam epitaxy (MBE), and it is incorporated at very high concentrations (~10^{20} cm^{-3}), well in excess of its solid solubility at typical annealing temperatures. As a result, there will be a thermodynamic driving force for a precipitating process. Absent any kinetic barriers, precipitation would lead to the formation of silicon carbide (SiC). However, even at high carbon concentrations, the extremely high SiC-Si interface energy makes the carbon precipitation process highly unlikely [48]. Rather, several studies have suggested the formation of an alternate agglomeration of carbon atoms, consisting of immobile clusters of carbon atoms [13],[45],[48],[49]. This carbon clustering process is a diffusion-assisted process that occurs parallel to the diffusion of carbon and can finally lead to a change in the effective diffusivity of carbon [48]. It takes place when a migrating C_i atom meets a C_s atom along its path, especially in carbon-rich regions, and forms the C_iC_s immobile pair. The clustering mechanism can be described by the following equations:

$$C_s + I \Leftrightarrow C_i, \tag{16}$$

$$C_i + C_s \Leftrightarrow C_iC_s, \tag{17}$$

thereby reducing the free C_i atoms, and the subsequent release of free interstitials through the reverse kick-out reaction.

2.5 Impact of Carbon Profile on Boron Diffusion Retardation and Device Performance

As mentioned in Chapter 1, the SiGe HBT is one of the key application areas for the use of carbon to reduce boron diffusion and improve device performance. In n-Si/p$^+$-SiGe/n-Si HBTs, boron outdiffusion from the base into the n-Si emitter and collector leads to the formation of parasitic barriers in the conduction band (Figure 7).

These parasitic barriers impede the flow of electrons from the emitter to the collector and are highly dependent on the boron concentration that diffuses into the silicon [50]. Small amounts of boron diffusion can be hard to detect by SIMS. However, the device itself is extremely sensitive to boron outdiffusion; small amounts of boron outdiffusion can cause large parasitic barriers for electrons at both heterojunctions. For example, Prinz *et al.* observed that an outdiffusion length of 25 Å caused a parasitic barrier of height 80 meV at the base-emitter junction [10]. This results in reducing the collector current, which has an exponential dependence on the barrier height. HBTs have therefore been employed as ideal probes to examine the effect of carbon incorporation on boron diffusion, as well as providing the fundamental motivation for developing this process. HBT electrical characteristics can be used to quantitatively compare boron diffusion in SiGe to boron diffusion in SiGeC under equilibrium diffusion conditions as well as diffusion enhanced by implant damage. Boron outdiffusion is clear in the reduction of the collector current for given bias conditions and the reduction of the Early voltage.

Lanzerotti *et al.* studied the common-emitter characteristics of transistors with and without localized substitutional carbon following arsenic implantation and annealing at 647 °C [9] (Figure 8). The transistors without carbon demonstrated a reduction in the collector current and Early voltage, indicating that boron has outdiffused even though the annealing conditions are far below the typical emitter thermal budget.

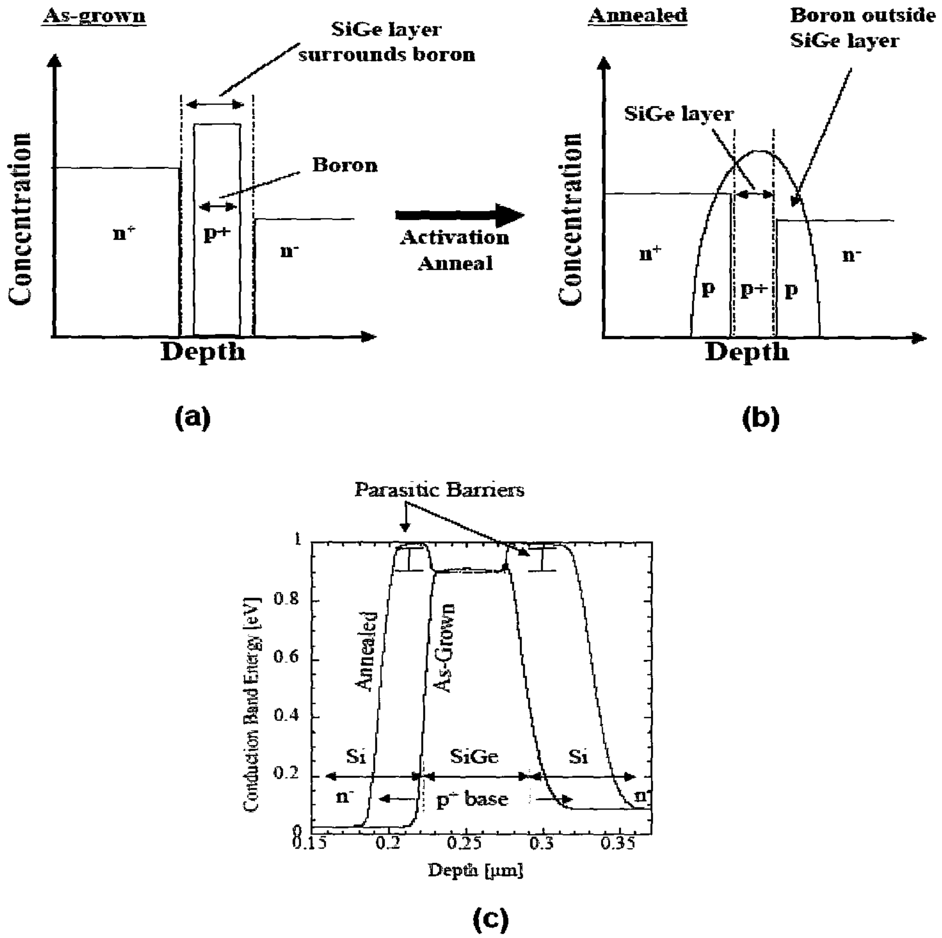

(a) (b)

(c)

Figure 7: Schematic diagram of (a) as-grown dopant profiles of a SiGe HBT, (b) base profile after annealing showing boron outdiffusion, and (c) conduction band diagram of the as-grown and annealed HBT showing the parasitic conduction band barriers created due to boron outdiffusion [50].

It is possible to fabricate HBTs using entirely epitaxial techniques such that dopants are introduced during growth. For such devices, what is of interest is the behavior of boron and carbon during inert anneals under conditions of point defect equilibrium. This type of process has been the subject of several studies (See, e.g., [12],[46],[51],[52]). Additionally, HBTs may be part of a BiCMOS process where implant damage and point defect non-equilibrium plays a role. Hence, several studies have focused on the role of carbon in reducing boron diffusion in implanted or oxidized samples [9],[13],[15],[53].

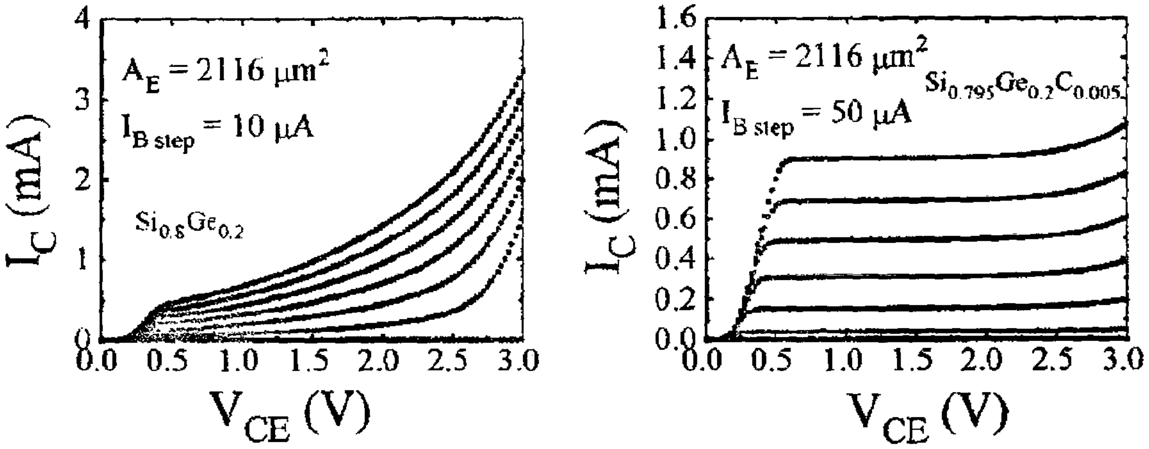

Figure 8: Common-emitter characteristics of transistors without (left) and with (right) a localized carbon concentration following As implantation and annealing at 647 °C [9].

Another factor of great interest in device design, as well as in better understanding the physics of the role played by carbon, is the carbon profile in the Si or SiGe sample. In the case of an initial uniform carbon distribution, and assuming a supersaturation of interstitials, continuous exchange between C and Si self-interstitials takes place. As a result, excess Si interstitials in a particular region result in an excess concentration of C_i in that region and a net transport of carbon results away from the region of excess interstitials (ion-implant region). Since the kick-out process eliminates Si interstitials as it generates C_i atoms, the excess interstitial concentration in the damage region is reduced by this process, and the enhancement to boron diffusion is also reduced.

If the carbon concentration is non-uniform, then one has to take into account the diffusion of the C_i out of the carbon rich region and the resulting effective Si interstitial flux out of that region. This will clearly have an effect on boron diffusion away from the C-rich region.

Finally, if C concentration is sufficiently high then C clustering effects come into play. These increase the efficiency of C in eliminating or trapping Si interstitials and must be accounted for in modeling the resultant boron diffusion. This happens by holding C_i atoms in immobile clusters, thus reducing the reverse kick-out reaction and the subsequent release of silicon interstitials.

In the following chapters we discuss the detailed modeling of these phenomena and examine the success of these models in explaining a wide range of experiments.

Chapter 3

EXISTING APPROACHES FOR MODELING CARBON DIFFUSION

Boron diffusion in Si and SiGe has been extensively researched and modeled in literature, and is generally considered well established. However, there exist several methods and regimes for modeling carbon diffusion based on subsets of experimental data. It is generally agreed that carbon dissolves in silicon substitutionally and that the diffusion of carbon occurs through a substitutional-interstitial mechanism. However, there is little agreement on a modeling scheme for the carbon behavior, and on the mechanisms taken into account to model carbon diffusion. Moreover, many studies use established diffusion parameters for carbon based on diffusion experiments, while some extract their own diffusion parameters.

In this chapter we present the existing approaches by several groups to model carbon diffusion and, hence the subsequent effect on suppressing boron diffusion in Si and SiGe. We start by presenting an analysis of the diffusion parameters involved in modeling the diffusion of B and C in Si and SiGe based on existing studies.

3.1 Review of Diffusion Parameters

3.1.1 Silicon Self-Diffusion Parameters

Among the uncertain factors for the accurate modeling of interstitial and vacancy mediated diffusants are the individual magnitudes of the silicon self-diffusion components; namely the diffusion coefficients (D_I, D_V) and the equilibrium concentrations (C_I^*, C_V^*) of the $D_I C_I^*$ and $D_V C_V^*$ components.

Reasonably consistent values for the self-diffusion components have been reported in the literature [39]. Literature values for $D_I C_I^*$ [54],[55],[56],[57] are used in most of the studies presented later in this chapter with considerable agreement; Figure 9 shows the literature values reported by Bracht *et al.* [54] and Ural *et al.* [55], and the FLOOPS-ISE default for the silicon interstitial self-diffusion component normalized to the Si atom density (C_0=5×10^{22} cm^{-3}). The FLOOPS-ISE values for the silicon self-diffusion come from *ab initio* calculations. As well, Figure 10 shows good agreement between literature values by Bracht *et. al.* [58] and Ural *et al.* [55] for the normalized $D_V C_V^*$ component that were reported in studies involving B and C diffusion in Si and/or SiGe.

The $D_I C_I^*$ and $D_V C_V^*$ indicate respectively the contribution of interstitials and vacancies to Si self-diffusion. Figures 9 and 10 demonstrate that there is considerable agreement on the value of each of these products. However, several experiments have been conducted, including ones involving carbon diffusion, where the separate values of

D_I (or D_V) and C_I^* (or C_V^*) affects the final outcome. In modeling such experiments, the individual values are used as fitting parameters.

Figures 11 and 12, show a comparison between different values for each of the diffusivity, D, and solubility, C^*, for interstitials (Figure 11) and vacancies (Figure 12). The comparison is made between the default values in FLOOPS-ISE and values extracted from several C diffusion studies where these values were used as fitting parameters while keeping the two products, $D_I C_I^*$ and $D_V C_V^*$, constant. A wider spread is evident in the vacancy component factors compared to the interstitial component factors.

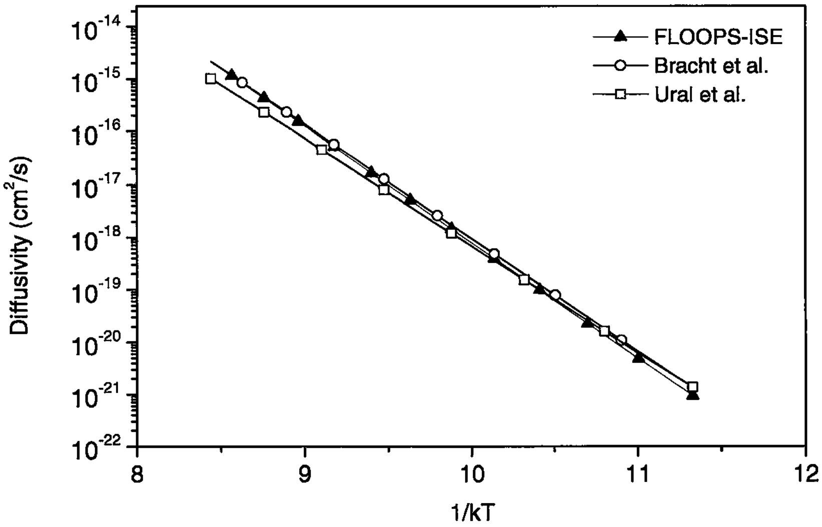

Figure 9: The FLOOPS-ISE and literature values (Refs. [54] and [55] respectively) for the silicon interstitial self-diffusion component.

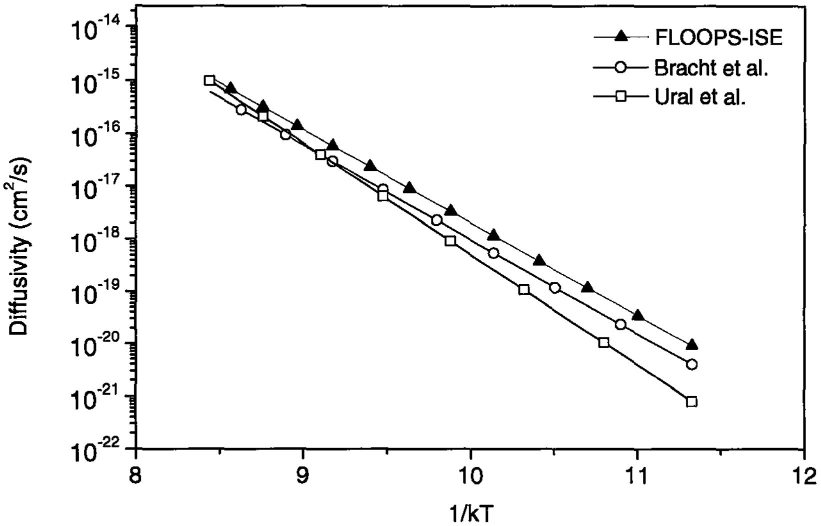

Figure 10: The FLOOPS-ISE and literature values (Refs. [58] and [55] respectively) for the silicon vacancy self-diffusion component.

3.1.1.1 Effect of Ge and C on Silicon Self-Diffusion Parameters

It is known that the equilibrium concentrations of interstitials and vacancies increase with the presence of Ge [61],[62]. Additionally, the compressive strain due to Ge increases C_V^* and decreases C_I^*, and the tensile strain has the opposite effect on the point-defect equilibrium concentrations [61],[62]. The effect of carbon on these parameters is unknown. These effects are however generally ignored in studies relevant to this work.

3.1.2 Boron Diffusion Parameters

As mentioned earlier, B diffusivity in Si is well-established and modeled, and there is general agreement that the presence of Ge retards B diffusion. As a result, the B diffusivity value was not reported in most of the studies presented in this chapter that characterize boron diffusion suppression due to C. Figure 13 presents the intrinsic B diffusivity in Si comparing it with values taken from literature.

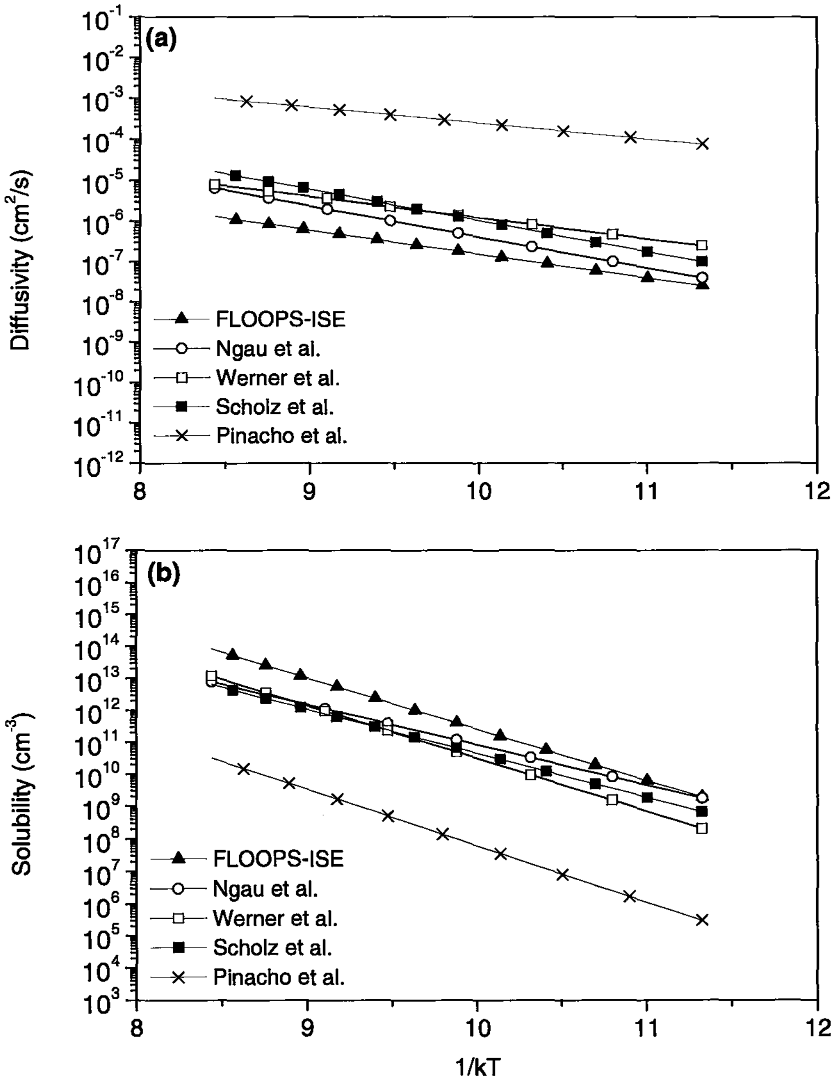

Figure 11: Interstitial diffusivities (a), and equilibrium concentrations (b) of FLOOPS-ISE and as reported by [13], [59], [60], and [48] respectively.

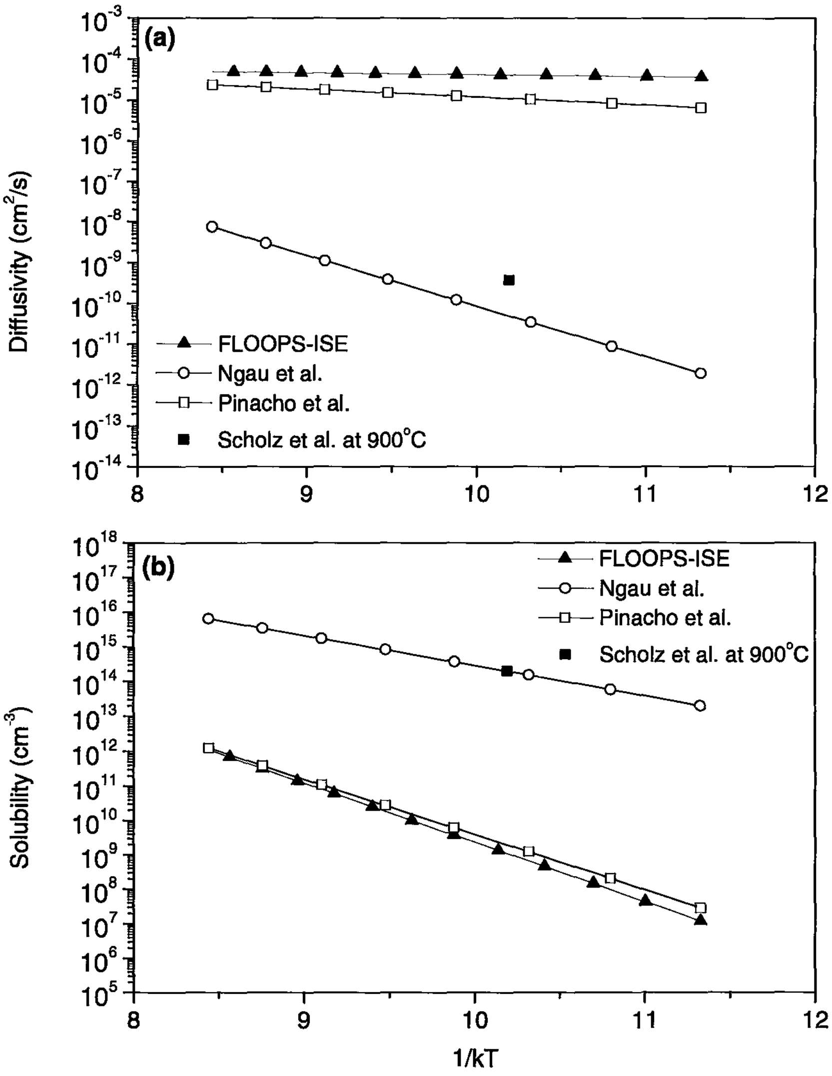

Figure 12: Vacancy diffusivities (a), and equilibrium concentrations (b) of FLOOPS-ISE and as reported by [13], [48], and [60] respectively.

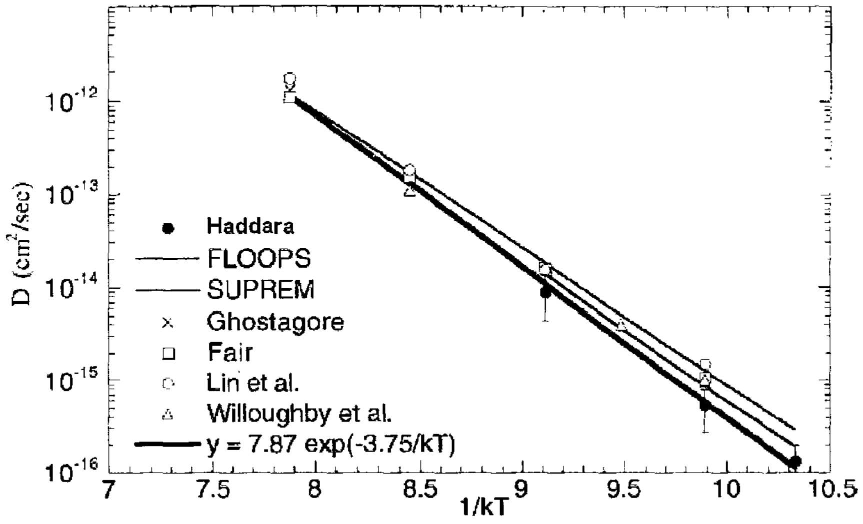

Figure 13: Study by Haddara *et al.* determining boron intrinsic diffusivity and comparing results with previous work [63].

3.1.3 Carbon Diffusion Parameters

Consistent carbon transport parameters taken from literature have been used in most of the studies for modeling C diffusion (See e.g., [13],[59],[60],[64],[65]). Table II lists these values for the effective equilibrium carbon diffusivity $D_{C_s}^{\text{eff}}$, the carbon solubility $C_{C_s}^{\text{eq}}$, the interstitial carbon solubility $C_{C_i}^{\text{eq}}$, and the interstitial carbon diffusivity D_{C_i}, where $D_{C_s}^{\text{eff}} = D_{C_i} C_{C_i}^{\text{eq}} / C_{C_s}^{\text{eq}}$.

Table II: Literature values for C transport parameters that are used in several studies.

Parameter	Prefactor	Activation Energy (eV)	Reference
$D_{C_s}^{\text{eff}}$	0.95 cm^2/s	3.04	[44]
$C_{C_s}^{\text{eq}}$	4×10^{24} cm^{-3}	2.30	[66]
D_{C_i}	0.44 cm^2/s	0.87	[67]
$C_{C_i}^{\text{eq}}$	8.64×10^{24} cm^{-3}	4.47	[47]

In a recent study, Sibaja-Hernandez *et al.* [12] investigated B and C diffusion in a SiGe layer and extracted a value for $D_{C_s}^{\mathrm{eff}}$. A comparison between their value, the value reported in Table II, and other well-established literature values for the equilibrium carbon diffusivity, as given in Figure 14, shows that their value deviates from the other literature values one order of magnitude.

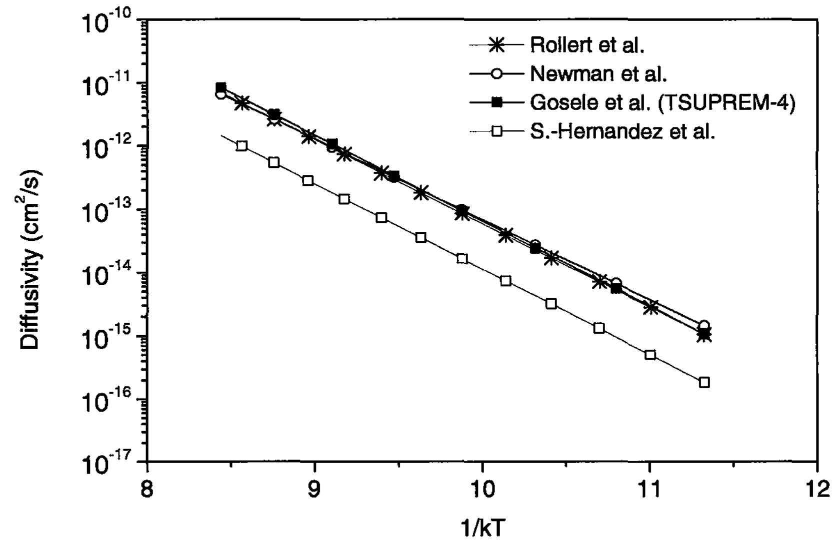

Figure 14: Comparison between the equilibrium carbon diffusivity according to [44], [68], [47], and [12], respectively.

3.2 Different Modeling Approaches

Note: In the remainder of this chapter, wherever we state that values are taken "from the literature" we refer to the values reported in the foregoing section. Where there are significant differences between studies reported above, we specify the source.

3.2.1 Kick-out Mechanism Only

Scholz *et al.* have studied carbon diffusion in terms of the kick-out mechanism only [64]. They demonstrated with simulations that the diffusion of carbon incorporated in silicon at concentrations above its solid solubility will induce an undersaturation of silicon self-interstitials, and simulated its impact on boron diffusion using the kick-out reaction constant as a fitting parameter. Carbon diffusion data and the $D_I C_I^*$ value were obtained from the literature. Furthermore, they argued that the carbon clustering reaction need not be taken into account

In addition, Werner *et al.* have also suggested the kick-out mechanism only for carbon diffusion. They investigated diffusion of a superlattice structure of carbon spikes (carbon concentration above solid solubility limit at the annealing temperature), after annealing in the range of 680-850 °C [59]. The carbon diffusion parameters $D_{C_s}^{\mathrm{eff}}$, D_{C_i}, and $C_{C_s}^{\mathrm{eq}}$ were obtained from literature, and $C_{C_i}^{\mathrm{eq}}$ was determined from $D_{C_s}^{\mathrm{eff}} = D_{C_i} C_{C_i}^{\mathrm{eq}} / C_{C_s}^{\mathrm{eq}}$. The silicon interstitial self-diffusion data were also taken from. With no free parameters for the simulation, they determined the kick-out reaction constant to be $9.3\times10^4 * \exp(-1.63\mathrm{eV}/kT)$. However, the simulations using only the kick-out reaction underestimated carbon diffusion at temperatures above 800 °C. The observed discrepancies between simulation and experiment were attributed to the following effects: (1) a simple form of precipitation taking place via carbon clustering, (2) accuracy of the parameters describing carbon diffusion, and (3) vacancies contributing to the diffusion of carbon through the dissociative or Frank-Turnbull mechanism. To address this, the authors experimented with several parameters. Increasing D_{C_i} had an equal and opposite effect on $C_{C_i}^{\text{eq}}$, which was determined by $C_{C_i}^{\text{eq}} = C_{C_s}^{\text{eq}} D_{C_s}^{\text{eff}} / D_{C_i}$, so there was no net influence on the carbon diffusion since $D_{C_s}^{\text{eff}} = D_{C_i} C_{C_i}^{\text{eq}} / C_{C_s}^{\text{eq}}$. Better correspondence between simulation and experiment was obtained by increasing the C_{C_i} concentration via increasing either D_I or C_I^* in the self-diffusion coefficient $D_I C_I^*$ by a factor of 2 beyond literature value for $D_I C_I^*$. This increase is well within the error bar of the data on $D_I C_I^*$ [54]. In addition, they reported that the inclusion of the dissociative mechanism in the model showed no significant influence on the diffusion profiles based on literature values for the vacancy diffusivity, D_V, and equilibrium concentration, C_V^*. However, better fits between simulation and experiment were obtained by increasing the vacancy diffusivity, D_V, while keeping the product $D_V C_V^*$ constant.

3.2.2 Kick-out and Clustering Mechanisms

Several groups have argued that while the kick-out mechanism by itself is not sufficient to model the diffusion of carbon and its effect on boron, it would be adequate to take into account the carbon clustering reaction in addition to the kick-out reaction [49],[65],[69]. Rücker *et al.* investigated diffusion of boron spikes in epitaxial silicon with and without carbon background doping of 10^{20} cm^{-3} [69]. Carbon doped samples demonstrated suppressed boron diffusion compared to samples without a background carbon doping after annealing at 900 °C. The authors computed a value for C_I^* in carbon-rich crystals assuming a large binding energy (1.45 eV) for the interstitial carbon atom (C_i) formed via the kick-out reaction. In addition, they suggested that carbon clusters act as interstitial sinks for cases of interstitial supersaturation (ion-implantation). Assuming one interstitial atom is consumed per carbon cluster, an estimate for the rate constant of carbon precipitation, and consequently for the rate of interstitial annihilation, was computed from the thermal stability of $Si_{1-x}C_x$ alloys. Unlike later studies by the same group, this approach is somehow *ad hoc* and does not reflect the physics of the individual mechanisms involved.

In a later work, Rücker *et al.* again investigated B diffusion suppression by C using the kick-out and clustering mechanisms for carbon diffusion, and the kick-out mechanism for B diffusion [65]. In contrast to their first study reported above, they solved a system of partial differential equations for kick-out diffusion assuming local equilibrium is established. The total C concentration was divided into concentrations of C_s, C_i, and a fraction for C-rich clusters of a not identified microscopic structure. The test structure consisted of a boron doping superlattice with an inhomogeneous carbon distribution that underwent annealing at 900 °C for 45 min, as illustrated in Figure 15. Boron diffusion was strongly suppressed in the C-rich region compared to the adjacent C-poor region. In their simulations, the silicon interstitial self diffusion component $D_I C_I^*$, and the carbon diffusion parameters corresponded to literature values. They reported that the individual values of D_I and C_I^* are of minor importance. As pointed out in Figure 15, when C diffusion was modeled using the kick-out mechanism only, insufficient carbon diffusion was predicted out of the C-rich layer. This demonstrates that given the known magnitude of the silicon interstitial self-diffusion component, $D_I C_I^*$, the interstitial flux into the C-rich region is insufficient to maintain a flux of C_i out of that region sufficiently large to explain the measured data. It was suggested that the flux of carbon could be due to emission of additional C_i from C-rich clusters. To overcome the discrepancy between simulation and experiment, an initial concentration of C clusters was assumed to dissolve at a constant rate, releasing C_i atoms that contribute to the diffusion of carbon.

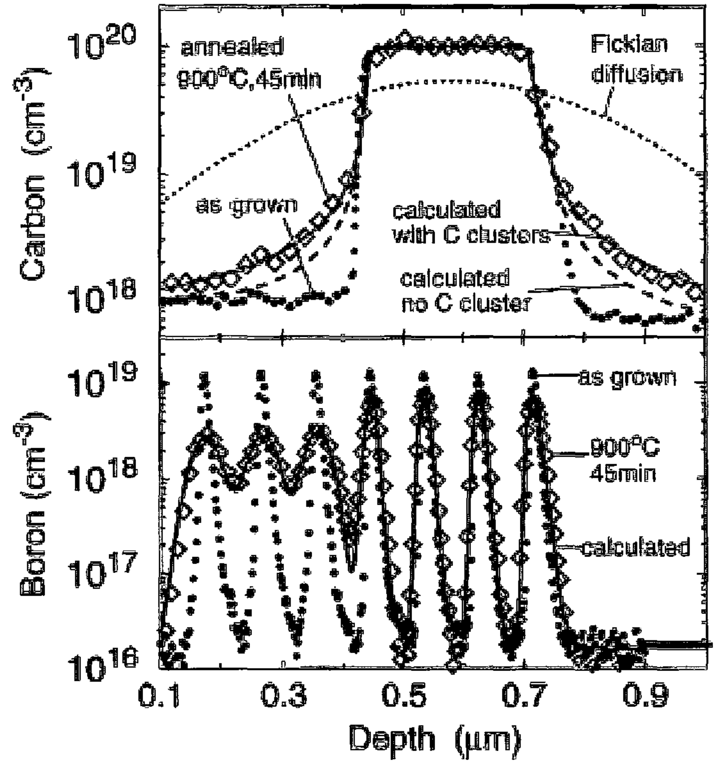

Figure 15: As-grown profiles (full circles), SIMS profiles (open diamonds) and simulated profiles (solid lines) of a carbon (top) and boron (bottom) doped sample undergoing a thermal budget of 900 °C, 45 min. The solid line in the top figure represents carbon simulation due to kick-out and including the emission of interstitial carbon from C-rich carbon clusters, while the dashed line represents the simulation without the clustering. Fickian diffusion is represented in dotted line [65].

3.2.3 Kick-out and Frank-Turnbull Mechanisms

Rather than including the clustering reaction, several groups adopted the approach of including the Frank-Turnbull (dissociative) mechanism in addition to the kick-out reaction [12],[46],[60],[51]. Scholz *et al.* [60] analyzed the same B doping superlattice sample reported by Rücker *et al.* [65] that was discussed in the previous section (Figure 15). In contrast to Rücker *et al.*, Scholz *et al.* suggested that the influence of vacancies should be taken into account, and that carbon diffusion profiles can be accurately simulated assuming that both the kick-out and Frank-Turnbull mechanisms operate simultaneously, and excluding the carbon clustering. For the simulations, the carbon diffusion parameters $D_{C_s}^{\mathrm{eff}}$, D_{C_i}, and $C_{C_s}^{\mathrm{eq}}$ were obtained from the literature, and $C_{C_i}^{\mathrm{eq}}$ was determined from $D_{C_s}^{\mathrm{eff}} = D_{C_i} C_{C_i}^{\mathrm{eq}} / C_{C_s}^{\mathrm{eq}}$. The silicon interstitial diffusivity D_I and equilibrium concentration C_I^* were also taken from [54], as the authors assumed a diffusion-limited forward reaction rate for the kick-out reaction given by $k_{\mathrm{KO}} = 4\pi r D_I$, where r is the capture radius, and used the mass action law to compute the reverse rate. For the Frank-Turnbull reaction, they used the splitting of the vacancy self-diffusion component $D_V C_V^*$ into its two factors, C_V^* and D_V, while keeping the product constant, as the only fitting parameter at 900 °C. The value for the product $D_V C_V^*$ was obtained from the literature. They determined the individual values from C outdiffusion profiles, which are sensitive to D_V, suggesting that this sensitivity is associated with the formation of a supersaturation of vacancies in C-rich regions due to the outdiffusion of carbon by the Frank-Turnbull mechanism.

In later studies Rücker *et al.* followed the approach of the kick-out and Frank-Turnbull mechanisms, while excluding the clustering reaction [46],[51]. Local equilibrium was assumed for the kick-out reaction, while the rate of the Frank-Turnbull reaction was determined from measured outdiffusion profiles of carbon following Scholz *et al.* [60]. However, in a study on the impact of carbon on transient enhanced diffusion of boron, it was suggested that the Frank-Turnbull mechanism plays a minor role in the case of high interstitial concentrations [53].

Sibaja-Hernandez *et al.* have also accounted for C diffusion according to the kick-out and Frank-Turnbull mechanisms only in a very recent study [12]. In their work, B, C and Ge diffusion profiles were characterized in a SiGeC region due to an RTA step in the temperature range 1020-1070 °C, for 10 seconds under inert and oxidizing ambients. For the diffusion data they used the defaults of their process simulator (TSUPREM-4), which correspond to the values by Ural *et al.* [55] for the silicon self-diffusion as we have reported them in Section 3.1.1 above. For boron and carbon the TSUPREM-4 diffusion parameters correspond to values reported in Sections 3.1.2 and 3.1.3, respectively. The B diffusion was modified to account for the presence of Ge. The forward rates of the kick-out and Frank-Turnbull reactions for C diffusion were determined from $k_{f,\mathrm{KO}} = 4\pi r D_I$ and $k_{f,\mathrm{FT}} = 4\pi r(D_{C_i} + D_V)$, respectively. The reverse rates were calculated from $k_{r,\mathrm{KO}} = k_{f,\mathrm{KO}} C_I^{\mathrm{eq}} D_{C_i} / D_{C_s}^{\mathrm{eff}}$, and $k_{r,\mathrm{FT}} = k_{f,\mathrm{FT}} C_V^{\mathrm{eq}} D_{C_s}^{\mathrm{eff}} / D_{C_i}$. They used the values thus obtained for the reaction rates as a starting point, but then varied the reaction rates to obtain fits between simulation and experiment. Using this approach, they reported an extracted value for the equilibrium C diffusivity $D_{C_s}^{\mathrm{eff}}$. Their value is compared with literature in Figure 14.

3.2.4 Kick-out, Frank-Turnbull and Clustering Mechanisms

Ngau *et al.* [13] and Pinacho *et al.* [48] maintain that given both the experimental data, and the well-established parameters describing carbon diffusion, the kick-out, Frank-Turnbull, and carbon clustering reactions must all be included in an accurate, physically-based model. Ngau and co-workers investigated B and C diffusion in a sample that consists of two boron marker layers of 2×10^{18} cm^{-3} concentration and a $Si_{1-x-y}Ge_xC_y$ layer in between with x=9.6 % and y=0.037 %. The sample underwent ion-implantation and annealing at 750 °C for various times. In this study the effect of BICs and {311} defects associated with implantation were accounted for using the models in the TSUPREM-4 process simulator. For the BICs they followed the approach of modeling the B_3I cluster only, which is proposed as one of the more dominant large BICs [70], and which has previously been used to successfully fit B diffusion data from experiments under a variety of implant and anneal conditions [71]. For the {311} defects, they used the parameters given by Rafferty *et al.* [41]. In their simulations, carbon diffusion data was obtained from literature. As well, the silicon self-diffusion components $D_I C_I^*$, and $D_V C_V^*$ were taken from literature. The splitting of $D_I C_I^*$ was performed by fitting B diffusion profiles of reference samples without C; D_I was adjusted within the error given in literature, and C_I^* accordingly to keep their product constant. It was also reported that the separate values of $D_V C_V^*$, as long as the product is constant, did not have a significant impact on the B or C profiles in their experiments which involve high supersaturation of interstitials due to implantation. However, using a previous C outdiffusion experiment under inert conditions [46], they determined the individual values of D_V, C_V^* that yielded a vacancy supersaturation, where C_V^* was obtained from literature based on metal diffusion experiments, and D_V was calculated to maintain the $D_V C_V^*$ product. For C diffusion, the kick-out and Frank-Turnbull diffusion-limited forward reaction rates were assumed, and the reverse rates were calculated from the law of mass action. The forward and reverse rates of the carbon clustering reaction were used as fitting parameters at 750 °C. The clustering reverse rate, i.e. the cluster dissolution rate, was increased to simulate additional experiments at higher temperatures, with the tendency of increased breakup of $C_i C_s$ pairs at higher temperatures.

Pinacho *et al.* [48] performed Monte-Carlo simulations for carbon diffusion profiles at 850 and 900 °C in carbon-doping superlattice structures. Carbon diffusion was modeled by the kick-out and Frank-Turnbull mechanisms, in addition to the carbon clustering phenomena which was modeled by incorporating complex clustering paths to account for several carbon-interstitial formation/dissolution mechanisms. High order interactions involving C_s, C_i, I and V were considered to simulate the growth and dissolution of immobile clusters. In their study, a cluster is denoted $C_n I_m$, where n is the number of carbon atoms, and m is the total number of atoms occupying interstitial sites (either carbon or silicon). It is assumed that all possible configurations of a given pair (*m,n*) are equivalent. The initial process of the carbon clustering phenomena is in agreement with previous explanations, where a C_i atom migrates until it encounters a C_s along its path, and forms a C_iC_s immobile pair, which the authors denote C_2I such that $C_i + C_s \Leftrightarrow C_2I$. However, it is further suggested that the C_2I can possibly break up by emission of an I leaving an immobile C_2 cluster: $C_2I \Leftrightarrow C_2 + I$. Additionally, the C_nI_m interactions involve growing by trapping either I or C_i that are rapidly diffusing across the material, in addition to trapping a neighbor silicon atom placed in the lattice and releasing a V. To match their simulations, they assumed values for the interstitial and vacancy diffusivities and equilibrium concentrations (See Figures 11 and 12). Additionally they assumed a value for the interstitial diffusivity D_{C_i} that is ~2 orders of magnitude lower than the value listed in Table II. They further reported that, using a formation energy for V consistent with *ab-initio* calculations rather than experiments results in a high activation energy for the reverse Frank-Turnbull mechanism ($C_i + V \Leftrightarrow C_s$), so that it plays a minor role at the annealing temperatures they used.

3.2.5 Other Approaches

Cowern *et al.* simulated B TED suppression in B and C implanted samples after a Si implantation and anneals at 900 °C [72]. To calculate B diffusion, the effects of boron and carbon clusters were taken into account. They assumed that n_c interstitials are trapped per C atom and varied n_c to fit the diffusion profiles for B at 900 °C, assuming that all C atoms are considered as traps for interstitials ($n_c \geq 1$). While this model results in good fits for their particular experiments, it avoids a detailed explanation of the physical mechanisms responsible for the removal of interstitials (i.e. the number n_c is the result of the composite effect of the kick-out, Frank-Turnbull and carbon clustering reactions discussed above).

Rajendran *et al.* have performed simulations only for boron diffusion in a $Si_{1-x-y}Ge_xC_y$ layer under equilibrium conditions at 900 °C [52]. It was suggested that the retardation of B diffusion in C-rich regions is attributed to the deactivation of boron, which leads to a lower hole concentration. This results in a difference in the B diffusivity and boron flux. A simplified model for B diffusivity was modified to account for the Ge and C effects, assuming an activation energy for B in Si given by: $3.62+(0.4xy)\pm 0.0154$, where x and y are the fractional values (at.%) of Ge and C respectively. Furthermore, the local strain effect due to the presence of Ge and C was included by modifying the activation energy and the intrinsic carrier concentration. This model has not been tested against experimental data.

In a recent work by Mirabella and co-workers, boron and carbon diffusion were experimentally characterized under non-equilibrium conditions (ion-implantation) at 800 °C, to study the effect of substitutional carbon in a $Si_{1-y}C_y$ layer on the TED of B [45]. The $Si_{1-y}C_y$ layer is placed between a deep boron spike and the surface implanted region, and behaves as a filtering membrane for the interstitials flowing towards the bulk, thus reducing the boron TED. It is suggested that the effect of the layer on boron TED is dependent on the total carbon dose which is varied by varying the thickness of the layer. The effect of carbon was analyzed by solving the time and spatial evolution for the interstitial concentration and the interstitial trap concentration, where the trap density was suggested as the sum of a background of intrinsic traps (within the material) plus the carbon concentration in the $Si_{1-y}C_y$ layer. In their regime, carbon in the layer undergoes clustering rather than out-diffusion, suggesting that C can be considered as a nondiffusive trap; a forward kick-out reaction takes place ($C_s + I \rightarrow C_i$) where a substitutional C_s traps a self-interstitial I, producing a highly mobile interstitial carbon atom (C_i). The mobile C_i does not undergo an outdiffusion, but interacts with a substitutional C_s, thus stopping its motion and forming an immobile cluster ($C_i + C_s \rightarrow C_iC_s$). After the clustering process, carbon is not able to capture additional interstitials, and interstitials can freely pass through the C-rich layer. Furthermore, the clusters are assumed very stable, such that the reverse clustering reaction can be neglected. In this manner, by means of the trapping and clustering reactions, one self-interstitial is trapped and is able to deactivate two substitutional carbon traps. The carbon precipitation and the experimental absence of carbon outdiffusion were explained in terms of the high interstitial flux, which moves the kick-out and clustering reactions in the forward direction. This group performed numerical analyses for the interstitials trapping but did not fit their experimental results for B and C diffusion.

Chapter 4

A CONSISTENT AND COMPLETE MODEL FOR CARBON DIFFUSION AND ITS IMPACT ON BORON DIFFUSION

As previously mentioned, B diffusion in Si and SiGe has been extensively researched and modeled in the literature, and is generally considered well established. This study focuses in particular on modeling C diffusion and its effect on B behavior. There is general agreement that C dissolves in silicon substitutionally and that the diffusion of C occurs through a substitutional-interstitial mechanism. However, as previously discussed, several schemes and approaches have been developed for modeling C diffusion based on subsets of experimental data, with little agreement on a certain one model, and on the mechanisms for C diffusion. Additionally, while many studies used established parameters for C diffusion, others extracted their own diffusion parameters as discussed in Chapter 3.

In this chapter we present the physics-based model that we developed for B and C diffusion. In the developed model, we make use of the well-established data for B and C diffusion, and silicon self-diffusion. The model accounts for all common phenomena involving B and C in Si and SiGe; it was verified by simulating several test structures described in the literature, in addition to recent experiments that characterize B diffusion in a SiGeC region. The simulated structures cover the temperature range 750 - 1070 °C and include diffusion under equilibrium and non-equilibrium conditions.

4.1 Modeling Carbon Diffusion

To model C diffusion, we implemented the kick-out and Frank-Turnbull diffusion mechanisms, given by the following reactions, respectively:

$$C_s + I \Leftrightarrow C_i, \tag{18}$$

$$C_i + V \Leftrightarrow C_s, \tag{19}$$

where mobile C_i atoms are formed via the kick-out and the Frank-Turnbull reactions. Additionally, we accounted for the C clustering mechanism as described by:

$$C_i + C_s \Leftrightarrow C_iC_s, \tag{20}$$

where C_i atoms are captured in immobile carbon complex pairs (C_iC_s), which in turn results in reducing the reverse kick-out reaction and the subsequent release of Si interstitials.

The above reactions result in a set of coupled reaction-diffusion equations [13]:

$$\begin{aligned}\frac{\partial C_{C_i}}{\partial t} &= \nabla.\left(D_{C_i}\nabla C_{C_i}\right) + k_{f,\mathrm{KO}}C_{C_s}C_I - k_{r,\mathrm{KO}}C_{C_i}\\ &\quad - k_{f,\mathrm{FT}}C_{C_i}C_V + k_{r,\mathrm{FT}}C_{C_s}\\ &\quad - k_{f,\mathrm{CI}}C_{C_i}C_{C_s} + k_{r,\mathrm{CI}}C_{CI},\end{aligned} \tag{21}$$

$$\frac{\partial C_{C_s}}{\partial t} = -k_{f,\mathrm{KO}} C_{C_s} C_I + k_{r,\mathrm{KO}} C_{C_i}$$

$$+ k_{f,\mathrm{FT}} C_{C_i} C_V - k_{r,\mathrm{FT}} C_{C_s}$$

$$- k_{f,\mathrm{Cl}} C_{C_i} C_{C_s} + k_{r,\mathrm{Cl}} C_{Cl}, \tag{22}$$

$$\frac{\partial C_{Cl}}{\partial t} = k_{f,\mathrm{Cl}} C_{C_i} C_{C_s} - k_{r,\mathrm{Cl}} C_{Cl}, \tag{23}$$

where C_{Cl} denotes the C_iC_s concentration. In the above, the *k*'s are the reaction rate constants with the first index in the subscript referring to forward (*f*) or reverse (*r*), and the second index referring to the kick-out (KO), Frank-Turnbull (FT), or the clustering (Cl) reactions. The forward rates of the KO and FT reactions are determined under diffusion limited conditions by:

$$k_{f,\mathrm{KO}} = 4\pi r D_I, \quad k_{f,\mathrm{FT}} = 4\pi r (D_{C_i} + D_V), \tag{24}$$

where *r* is the capture radius and is equal to 0.5 nm. The KO and FT reverse reaction rates are estimated by law of mass action as:

$$k_{r,\mathrm{KO}} = k_{f,\mathrm{KO}} C_{C_s}^{\mathrm{eq}} C_I^{\mathrm{eq}} / C_{C_i}^{\mathrm{eq}},$$

$$k_{r,\mathrm{FT}} = k_{f,\mathrm{FT}} C_{C_i}^{\mathrm{eq}} C_V^{\mathrm{eq}} / C_{C_s}^{\mathrm{eq}}. \tag{25}$$

Additionally, and in contrast to previous attempts, we determined the forward rate for the clustering reaction under diffusion limited conditions:

$$k_{f,\mathrm{Cl}} = 4\pi r D_{C_i}, \tag{26}$$

and varied the reverse rate $k_{r,\mathrm{Cl}}$ as a fitting parameter, with the tendency of a higher reverse rate, i.e. higher dissolution of C_iC_s pairs, at higher temperatures. The above differential equations were then implemented in FLOOPS-ISE using the Alagator scripting language.

Finally the default point defect differential equations in FLOOPS-ISE were modified to incorporate the carbon diffusion by adding the terms: $-k_{f,\mathrm{KO}}C_{C_s}C_I + k_{r,\mathrm{KO}}C_{C_i}$, and $-k_{f,\mathrm{FT}}C_{C_i}C_V + k_{r,\mathrm{FT}}C_{C_s}$ to the right hand side of the continuity diffusion equations of the *I* and *V* respectively.

4.1.1 Carbon Diffusion Parameters

For C transport parameters we use the well-established values of Table II for the effective equilibrium carbon diffusivity $D_{C_s}^{\mathrm{eff}}$, carbon solubility $C_{C_s}^{\mathrm{eq}}$, interstitial carbon diffusivity D_{C_i}, and interstitial carbon solubility $C_{C_i}^{\mathrm{eq}}$, where $D_{C_s}^{\mathrm{eff}} = D_{C_i}C_{C_i}^{\mathrm{eq}} / C_{C_s}^{\mathrm{eq}}$.

4.2 Modeling Boron Diffusion

For B diffusion we implemented the pair diffusion model in FLOOPS-ISE. The basic assumption of most general FLOOPS-ISE diffusion models is that only dopant-defect pairs are mobile, while the substitutional (active) dopant atoms are immobile. FLOOPS-ISE solves the following equation for B diffusion:

$$\frac{\partial C_B}{\partial t} = \nabla(-J_B), \tag{27}$$

where the flux J_B includes fluxes of the different types of dopant-defect pairs; (B, I^0), (B, I^+), (B, V^0) and (B, V^+). A separate continuity equation is written to represent the diffusion of each dopant-defect pair. In general if it is assumed that a dopant diffuses with vacancies and interstitials, three different types of continuity equations are solved simultaneously – one each for the substitutional dopant, the dopant-interstitial pairs, and the dopant-vacancy pairs. These three sets of differential equations together with the two continuity equations for interstitials and vacancies describe the diffusion of the dopant through the interaction with vacancies and interstitials. This is referred to as the five-stream diffusion model. For a dopant A, the pair model is generally given by [73]:

$$-J_{A,\text{defect}} = \sum_c D_{A.\text{defect}^c} C_A \left(\frac{p}{n_i}\right)^c \left(\nabla \ln\left(C_A \frac{C_{\text{defect}}}{C^*_{\text{defect}}}\left(\frac{p}{n_i}\right)\right)\right), \tag{28}$$

where C_A is the substitutional dopant concentration, $J_{A,\text{defect}}$ is the diffusion flux of the dopant-defect pair, and $D_{A.\text{defect}^c}$ represents the diffusivities of the dopant-defect pairs at various charge states (c). In our case, the equilibrium boron diffusivity is given by:

$$D_B^{\text{eq}} = D_{B,I} + D_{B,V} = D_{B,I^0} + \frac{p}{n_i} D_{B,I^+} + D_{B,V^0} + \frac{p}{n_i} D_{B,V^+}, \tag{29}$$

such that $D_{B,I} = f_I \times D_B^{\text{eq}}$, and $D_{B.V} = (1-f_I)\times D_B^{\text{eq}}$, where B is known to have $f_I = 0.98$ [25], and its equilibrium diffusivity is known over a wide temperature range [63]. Table III lists the equilibrium boron diffusivity and the diffusivities of the boron-defect pairs that we implemented, the ratios of the boron-defect pairs diffusivities are the FLOOPS-ISE defaults.

Table III: Boron equilibrium diffusivity [63] and the diffusivities of the boron-defect pairs.

Parameter	Prefactor	Activation Energy (eV)
D_B^{eq}	7.87	3.75
D_{B,I^0}	0.98×4.3	3.75
D_{B,I^+}	0.98×3.57	3.75
D_{B,V^0}	0.02×4.3	3.75
D_{B,V^+}	0.02×3.57	3.75

4.2.1 Modeling Boron TED

To model the evolution of interstitial damage created by ion-implantation, hence TED, we implemented the "+1" model of FLOOPS-ISE. This model provides an estimate for the level of interstitials arising from the implant that contribute to the enhanced diffusion. A net imbalance in the ion-generated population of interstitials and vacancies is caused by implantation. At the early states of annealing, interstitials and vacancies recombine quickly to restore the lattice damage, leaving one atom per implanted ion which cannot be annealed out immediately. This one excess interstitial per ion ("+1" model) is thought to create the supersaturation of interstitials during TED [39].

Furthermore, we accounted for the effects of boron-interstitial-clusters and {311} defects, that are associated with TED. To model the BICs, we followed the simplified approach of using a single reaction to model the B_3I only [13],[71] which is proposed as one of the more dominant large BICs at high temperatures [70]. The BICs formation reaction is generally given by [13]:

$$n_B B + n_B p + n_f I \Leftrightarrow B_{n_B} I_{(n_f - n_r)} + n_r I \,, \tag{30}$$

such that BICs of size $B_{n_B} I_{(n_f - n_r)}$ are formed and n_r interstitials released when n_B boron atoms, n_B holes, and n_f interstitials react together. For the $B_3 I$, $n_B = 3$ and $(n_f - n_r) = 1$, and is modeled by the following equation [13]:

$$\frac{\partial C_{B_3 I}}{\partial t} = \frac{1}{\tau}\left[k_f n_i \left(\frac{C_B^{\text{active}}}{n_i}\right)^3 \left(\frac{n_i}{p}\right)^{-3} \left(\frac{C_I}{C_I^{\text{eq}}}\right)^{n_f} - C_{B_3 I}\left(\frac{C_I}{C_I^{\text{eq}}}\right)^{n_r}\right], \tag{31}$$

where C_B^{active} is the active boron concentration, k_f controls the amount of clustering, and τ controls the rate of clustering and declustering. The individual quantities n_f and n_r are interpreted as the average number of interstitials involved in the forward and reverse reactions of Eq. (30) respectively, and can be used together with k_f and τ as fitting parameters.

To model the {311} defects we used the FLOOPS-ISE defaults based on the model proposed by Law *et al.*, which computes the total number of interstitials in the defects (C_{311}) and the total number of defects (D_{311}) by solving the following equations [42]:

$$\frac{\partial C_{311}}{\partial t} = \frac{D_{311}\left(C_I - C_{311}^{\text{eq}}\right)}{\tau_{311}}, \tag{32}$$

$$\frac{\partial D_{311}}{\partial t} = \frac{-D_{311} C_{311}^{\text{eq}}}{\tau_{311}} \frac{D_{311}}{C_{311}}, \tag{33}$$

where τ represents the time constant.

4.3 Silicon Self-Diffusion

In a previous work [74], we used the defaults in FLOOPS-ISE for the silicon self-diffusion components, as well as the individual quantities of the *I* and *V* diffusivities and equilibrium concentrations, which come from *ab initio* calculations (Figures 9-12). In this work, we also use these values for the $D_I C_I^*$ and $D_V C_V^*$ components, and the individual values D_I and C_I^*. However, for the splitting of the $D_V C_V^*$ component into its two factors, in order to simulate all the experiments presented below we followed the approach by Ngau *et al.* [13], where C_V^* was based on results from metal diffusion experiments [54]. The vacancy diffusivity D_V was then calculated to maintain the $D_V C_V^*$ product. Table IV lists the silicon self-diffusion entities that we used in our model. Finally, the bulk recombination constant of *I* and *V* was estimated under diffusion limited conditions as $4\pi r(D_I + D_V)$.

Table IV: Silicon self-diffusion data used in our model.

Parameter	Prefactor	Activation Energy (eV)	Reference
$D_I C_I^*$	8262.6 cm^2/s	5.07	FLOOPS-ISE
$D_V C_V^*$	0.9562 cm^2/s	4.07	FLOOPS-ISE
D_I	0.138 cm^2/s	1.37	FLOOPS-ISE
C_I^*	2.99×10^{27} cm^{-3}	3.70	FLOOPS-ISE
C_V^*	1.4×10^{23} cm^{-3}	2.00	[54]
D_V	0.3415 cm^2/s	2.07	This work

Chapter 5

SIMULATION RESULTS AND DISCUSSION

In this chapter we present the simulation results obtained using the model and set of parameters described in Chapter 4. The model is validated against a range of published results.

5.1 Boron Diffusion Suppression by Carbon

5.1.1 Equilibrium Conditions

Figure 16 presents the experimental and simulated B and C profiles for our recent experiments that were obtained through collaboration [18]. The sample structure of Figure 16 consists of a boron spike occurring in a 40 nm $Si_{0.848}Ge_{0.15}C_{0.002}$ layer with a silicon cap layer (~150 nm) grown on top of the SiGeC layer; the as-grown C box profile has a peak concentration of 1.1×10^{20} cm^{-3}. For further details on sample preparation, refer to Ref. [12]. Different samples were subjected to RTA anneals at 1020, 1050, and 1070 °C for 10 s in N_2, with a ramp-up and ramp-down rates of 50 and 45 °C/s, respectively. For the three annealing temperatures, our model accurately captures the boron diffusion reduction due to the C as well as the effect of Ge which was included through the effective diffusivity of B by setting $D_B^{\mathrm{SiGe}} = 0.6 \times D_B^{\mathrm{Si}}$. In contrast to the simulations of Sibaja-Hernandez *et al.* [12] where the carbon clustering reaction was neglected (as discussed in Chapter 3), we demonstrate here that it is possible to use published values to simulate the diffusion of both C and B while taking into account all three mechanisms.

In Figure 17 we simulated the sample structure previously reported by Rücker *et al.* [65] and Scholz *et al.* [60] and consisting of a boron doping superlattice and an inhomogeneous C distribution with a peak concentration of 10^{20} cm^{-3}. Our model accurately predicts the diffusion of C and its impact on B which is evident through the significant diffusion reduction in the C-rich area compared to the C-poor area. As mentioned in Chapter 3, Rücker *et al.* ignored the FT reaction, while Scholz *et al.* ignored the carbon clustering reaction. Later in this chapter we show that the inclusion of the three reactions is necessary to successfully explain the diffusion behavior in other experiments. Figure 17 demonstrates that this experiment may also be modeled using the same set of equations and parameters necessary to simulate other results.

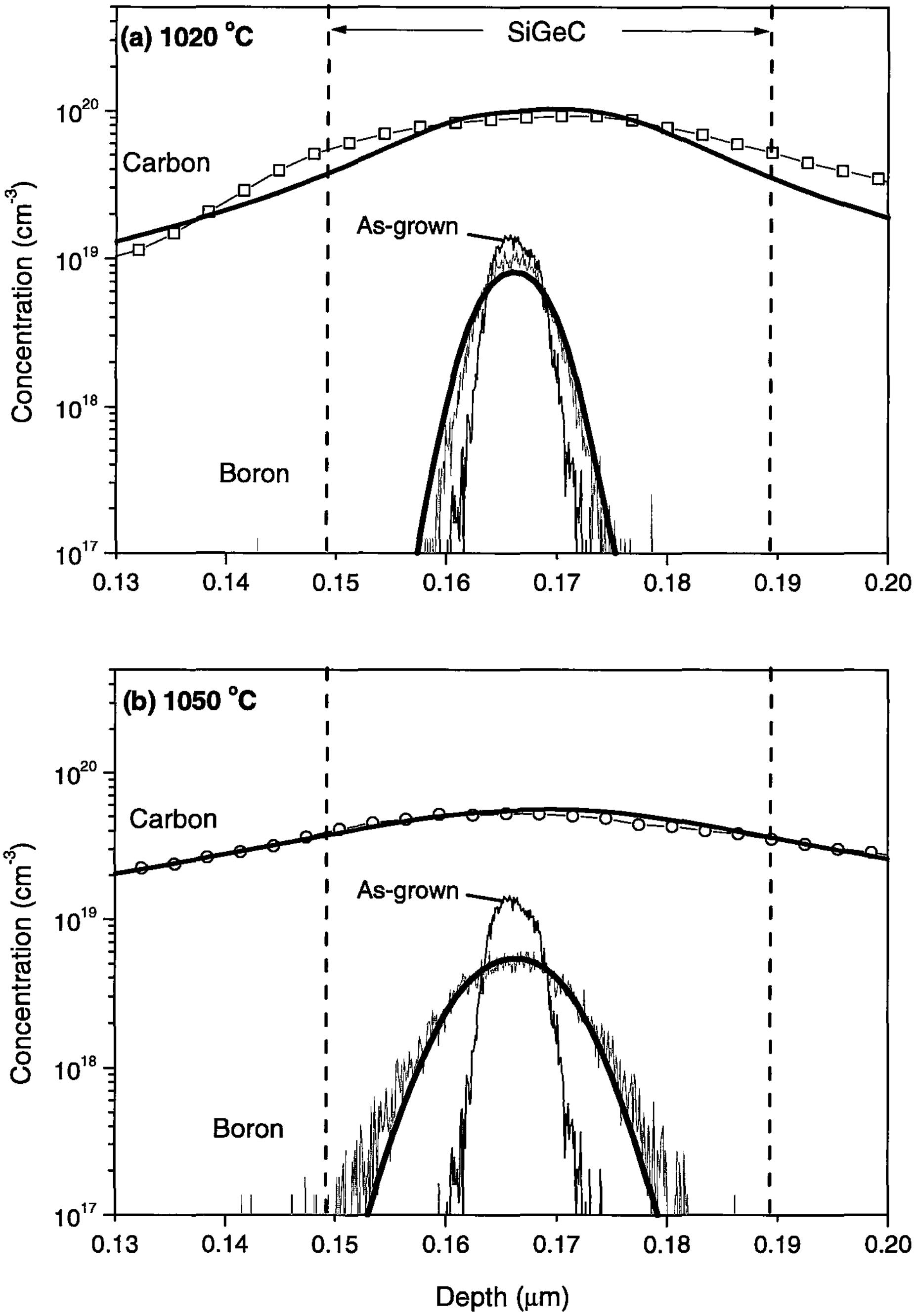
(a) 1020 °C
SiGeC
Carbon
As-grown
Boron
(b) 1050 °C
Carbon
As-grown
Boron
Concentration (cm^{-3})
10^{17}
10^{18}
10^{19}
10^{20}
0.13
0.14
0.15
0.16
0.17
0.18
0.19
0.20
Depth (μm)

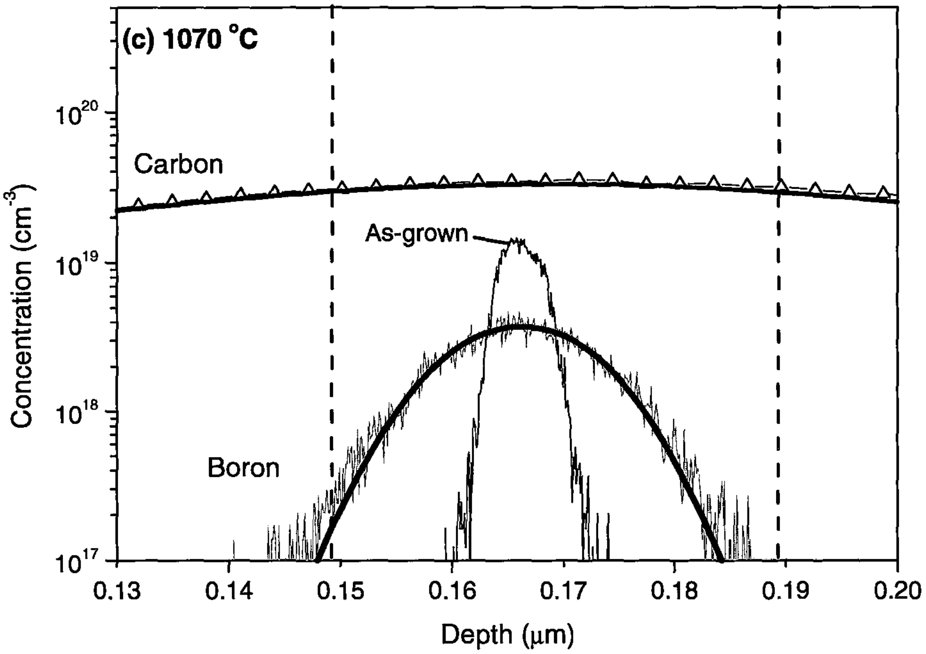

Figure 16: SIMS (symbols and gray scattered lines) and simulated (thick solid lines) profiles of B and C after inert RTA anneals of a boron spike in a $Si_{0.848}Ge_{0.15}C_{0.002}$ layer for 10 s at temperatures of: (a) 1020, (b) 1050, and (c) 1070 °C. The as-grown carbon box profile has a peak concentration of 1.1×10^{20} cm^{-3}.

Figure 18 presents a third experiment under equilibrium diffusion conditions for another structure reported by Rücker *et al.* [46]. The sample wafers were prepared with uniform B concentration in the surface region, and then an epitaxial layer with and without C doping (10^{20} cm^{-3}). Figure 18 shows the diffusion profiles for the samples with and without the C doping after a thermal budget of 900 °C for 2 hours in N_2, where the C doped sample shows reduced B diffusion compared to the no C sample.

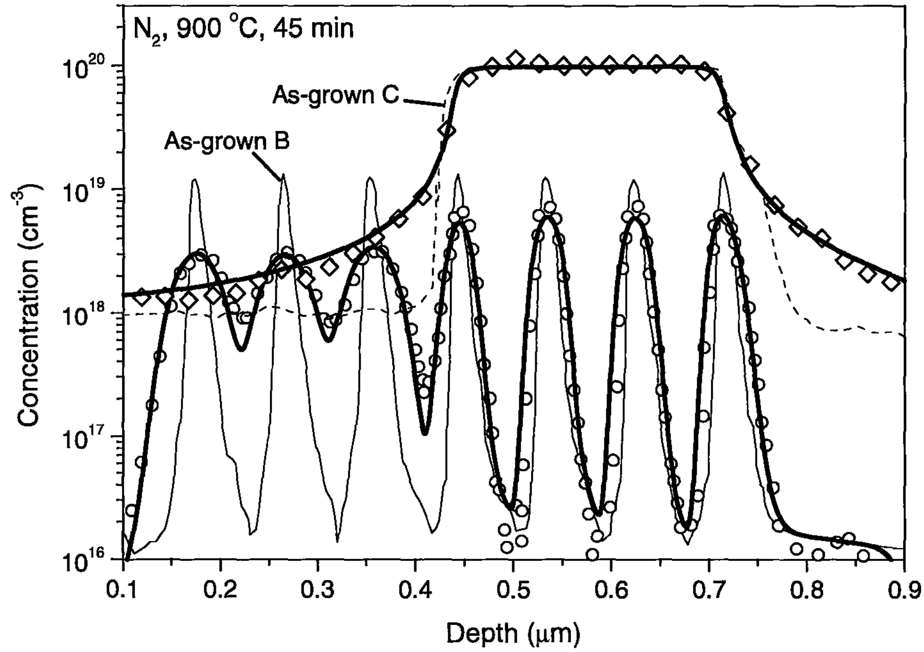

Figure 17: Comparison of our simulations (thick solid lines) for the diffusion of B spikes and C with the experimental annealed profiles (symbols) after a thermal budget of 900 °C, 45 min in N$_2$. Data extracted from Ref. [65].

5.1.2 Non-equilibrium Conditions

5.1.2.1 Boron Transient Enhanced Diffusion (TED)

In this section, we present simulation results for sample structures described in the literature that involve B TED. The first structure, as illustrated in Figure 19, was reported by Ngau *et al.* [13] and involves TED of two B marker layers in samples with and without a $Si_{1-x-y}Ge_xC_y$ layer (x=9.6% and y=0.037%) intervening the B marker layers. The presented sample underwent a 40 keV, 2.5×10^{13} cm^{-2} Si implant followed by a 4.25 minute anneal at 750 °C. Using the reference, Figure 19(a), that underwent implantation and annealing under the same conditions, we calibrated the boron diffusion and the BICs formation, with the following fitting parameters in Eq. (31) of the boron clustering:

$k_f = 1.24\times10^{-3}$, $\tau = 9.6\times10^{4}$, $n_f = 1$ and $n_r = 0$. As can be seen, in the SiGeC sample an immobile boron peak due to BICs formation is evident in the shallow marker layer, but not significant in the deeper marker layer, indicating that the C-rich region suppresses clustering by blocking interstitials from reaching the deeper B layer, which is well captured by our model.

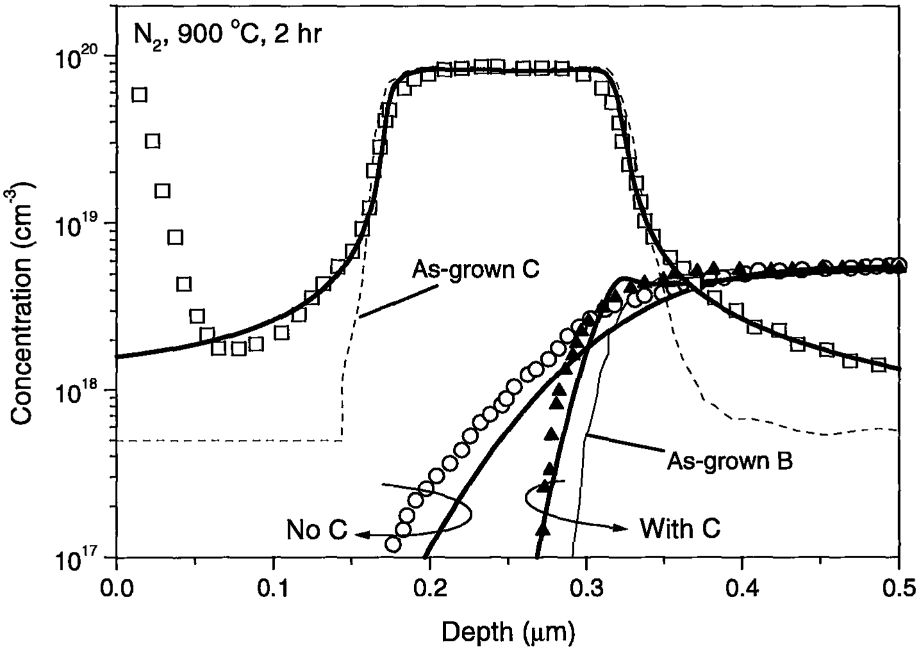

Figure 18: Diffusion of B from highly doped substrates in Si with and without C doping. Thick solid lines are the calculated profiles and symbols are SIMS data. Data extracted from Ref. [46].

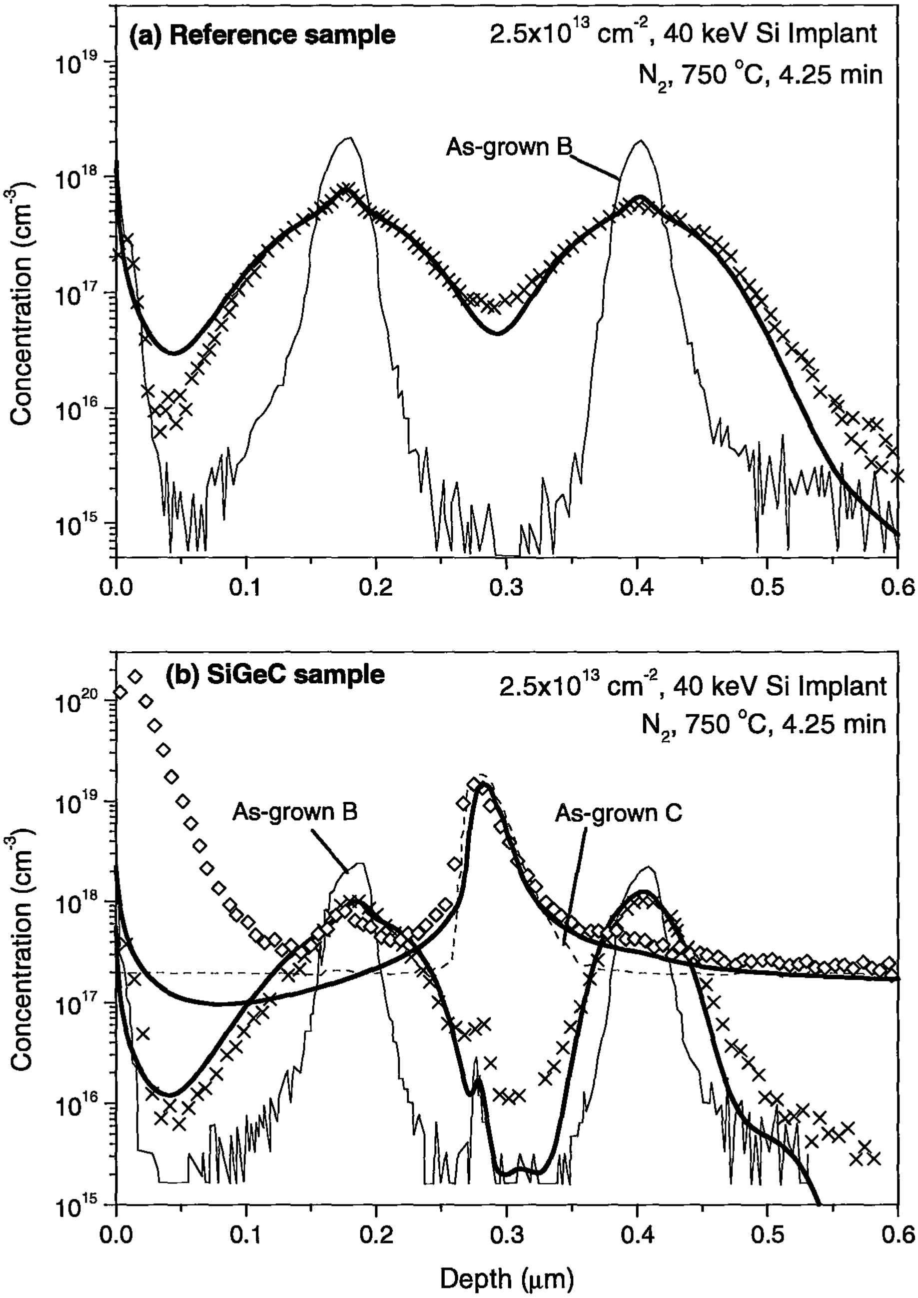

Figure 19: Simulations (thick solid lines) and annealed (symbols) profiles of B and C upon implantation and annealing of: (a) reference sample without C, and (b) sample with a SiGeC layer. Data extracted from Ref. [13].

The second sample involving B TED was reported by Mirabella *et al.* [45]. The structure, as shown in Figure 20, contains a B spike with a peak concentration of ~6×10^{18} cm^{-3} and inserted at a depth of 660 nm, while a $Si_{1-y}C_y$ layer (y=0.03%) was placed below a 200 nm Si cap layer and has a thickness of 250 nm. The sample underwent a 20 keV, 10^{14} cm^{-2} Si implant followed by annealing at 800 °C for 10 minutes. From comparison of B diffusion in the C-rich sample with the reference sample (without C), it is evident that the C acts as a trap for interstitials, thus preventing them from contributing to the enhanced B diffusion. The authors of this sample have reported that C outdiffusion was not evident in their experiments and have not reported C SIMS data for this sample. As mentioned in Chapter 3, they have explained the absence of C outdiffusion by suggesting that C in the C-rich layer undergoes clustering rather than out-diffusion; such that one Si interstitial deactivates two carbon atoms making C act as a nondiffusive trap. Using our model we successfully calculated the carbon effect in suppressing the B TED and the expected C behavior.

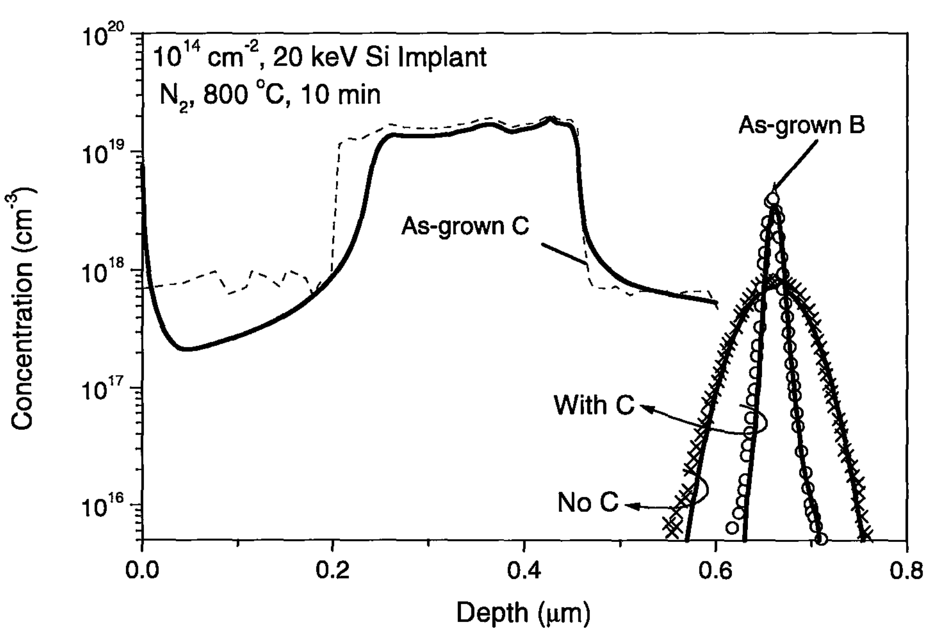

Figure 20: Complete suppression of B TED in Si due to a C-rich layer acting as trap for interstitials. Calculated and annealed profiles are plotted in thick solid lines and symbols respectively. Data extracted from Ref. [45].

In Figure 21 we used our model to simulate the suppression of B TED due to C in another experiment that was reported by Rücker *et al.* [53]. The sample structure is very similar to that of Figure 17; it consists of B doping spikes and a C concentration of ~5×10^{19} cm^{-3} located 450 nm below the surface. The sample in this case was implanted with BF$_2$ ions at an energy of 45 keV and a dose of 10^{14} cm^{-2}, and then annealed at 930 °C for 30 s in an inert ambient. Strongly suppressed B diffusion is observed in the C-rich region compared to the adjacent C-poor area.

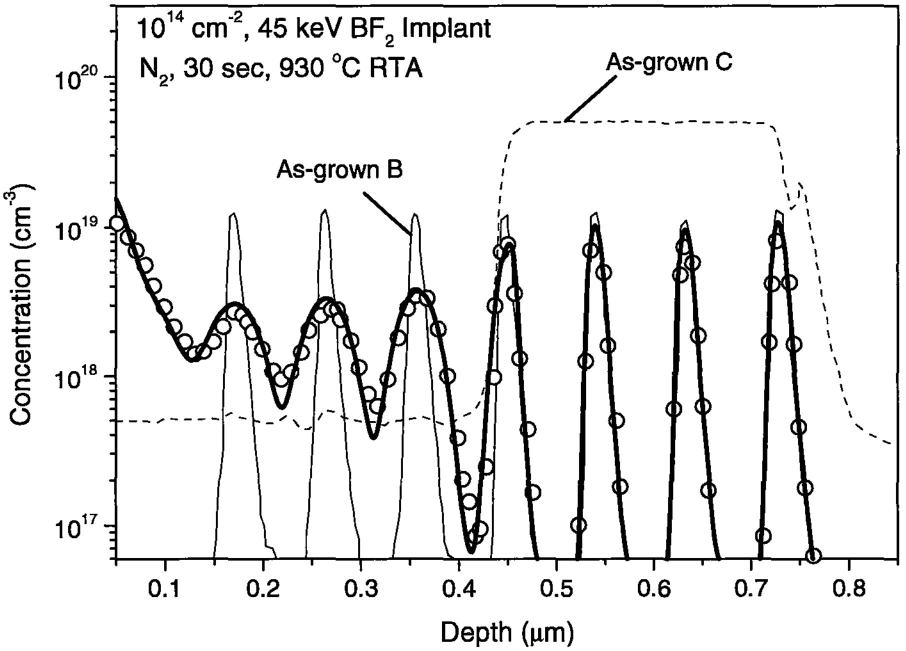

Figure 21: Simulated (thick solid line) and experimental (symbols) profiles of a B doping superlattice with a C-rich layer, upon implantation and annealing. Data extracted from Ref. [53].

In the above two samples we consider the effect of the {311} defects, however no B clustering was evident in the reported SIMS data.

5.1.2.2 Boron Oxidation Enhanced Diffusion (OED)

In this section, we use our model to verify the suppression of oxidation enhanced diffusion of B due to carbon incorporation by simulating two experiments that were reported by Carroll *et al.* [75],[76]. For the following OED experiments, B diffusion was calibrated according to reference samples that underwent similar experimental conditions.

As shown in Figure 22, an excellent match is obtained between simulation and experiment for the first OED suppression sample, which consists of four grown-in B peaks in Si, and a 20 nm $Si_{0.795}Ge_{0.2}C_{0.005}$ layer centered between the third and fourth B peaks at 675 nm below the surface. The SiGeC sample features reduced boron diffusion around the SiGeC layer compared to the reference sample, after annealing in O_2 at 850 °C for 30 minutes.

The second OED experiment underwent similar annealing conditions. The test structure consists of two B doped silicon layers with an intervening thin 25 nm $Si_{0.795}Ge_{0.2}C_{0.005}$ layer in between (Figure 23). Albeit some discrepancy between the simulation and the reported SIMS results, reasonable match is still obtained. In fact an inspection of the SIMS measurements reveals that the same dopant dose is not contained in the as-grown and annealed profiles, leading us to conclude that either the depth or the concentration scales were not properly calibrated in this particular experiment. Agreement with simulation is therefore limited to the overall trend in the data and the major features of the final profile. In particular, the simulated B profile accurately captures the "uphill diffusion" of the shallower boron peak that leads to the profile peak shifting deeper into the substrate. Additionally, the predicted broadening of the deep peak versus the shallower one is consistent with the experimental profile.

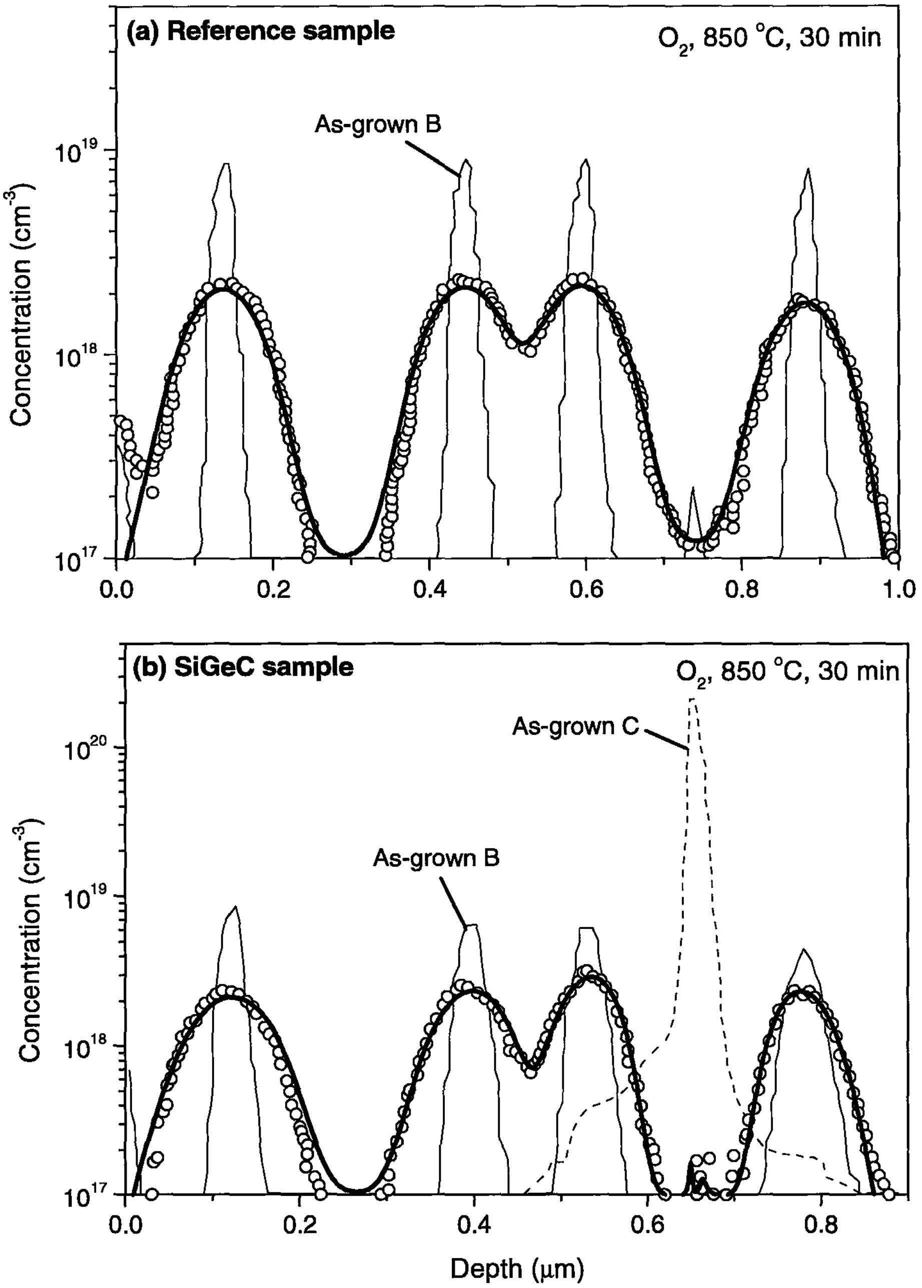

Figure 22: Comparison between simulation (thick solid line) and experiment (symbols) for B peaks diffusion without (a) and with (b) a $Si_{0.795}Ge_{0.2}C_{0.005}$ layer, after a thermal budget of 850 °C for 30 min in O_2. Data extracted from [75].

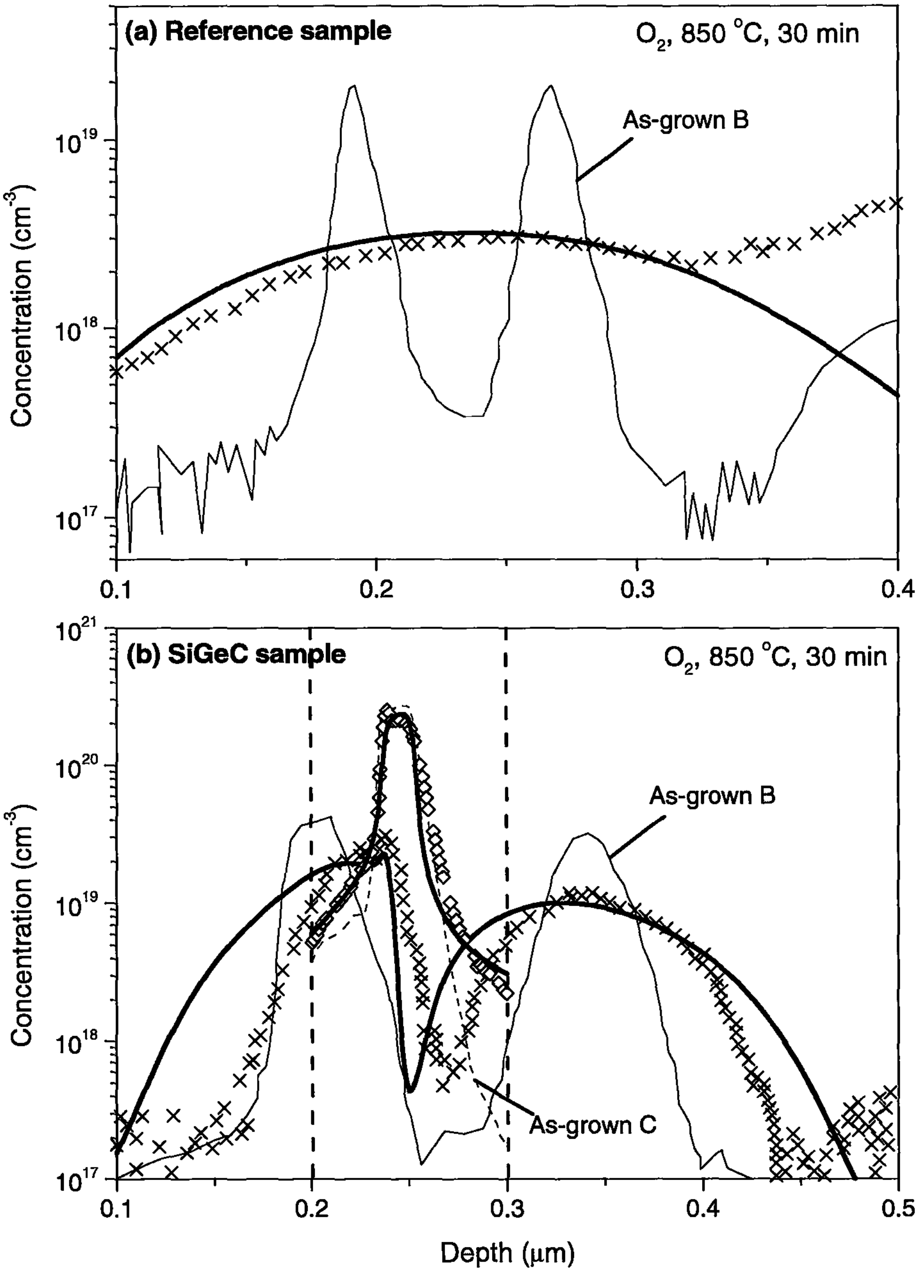

Figure 23: Boron OED suppression by a SiGeC layer intervening two boron-doped Si layers upon an oxide ambient anneal. Simulated and annealed profiles are plotted in thick solid lines and symbols respectively. Data extracted from Ref. [76].

5.2 Carbon Diffusion

To test our model for carbon diffusion only, we calculated the diffusion of C spikes in pure Si in a structure that was reported by Pinacho *et al.* [48], which is also similar to the structure by Werner *et al.* [59]. Similar to the widely studied B doping superlattice structures, the studied C structure consists of six C spikes, 10 nm wide, with a peak concentration of 2×10^{20} cm^{-3}, spaced 100 nm apart, and capped with 50 nm silicon. Figures 24 and 25 show the correspondence of simulation to the experimental profiles after an inert ambient anneal for different times at 850 and 900 °C, respectively. As discussed in Chapter 3, Pinacho *et al.* modeled C diffusion by the kick-out and Frank-Turnbull mechanisms, in addition to incorporating several complex carbon clustering paths, while Werner *et al.* implemented the kick-out mechanism only. Here we are able to model the published results using the same set of model equations and parameters that we have applied to all other results, i.e. we include the kick-out and Frank-Turnbull mechanisms in addition to modeling carbon-carbon clustering as a single reaction.

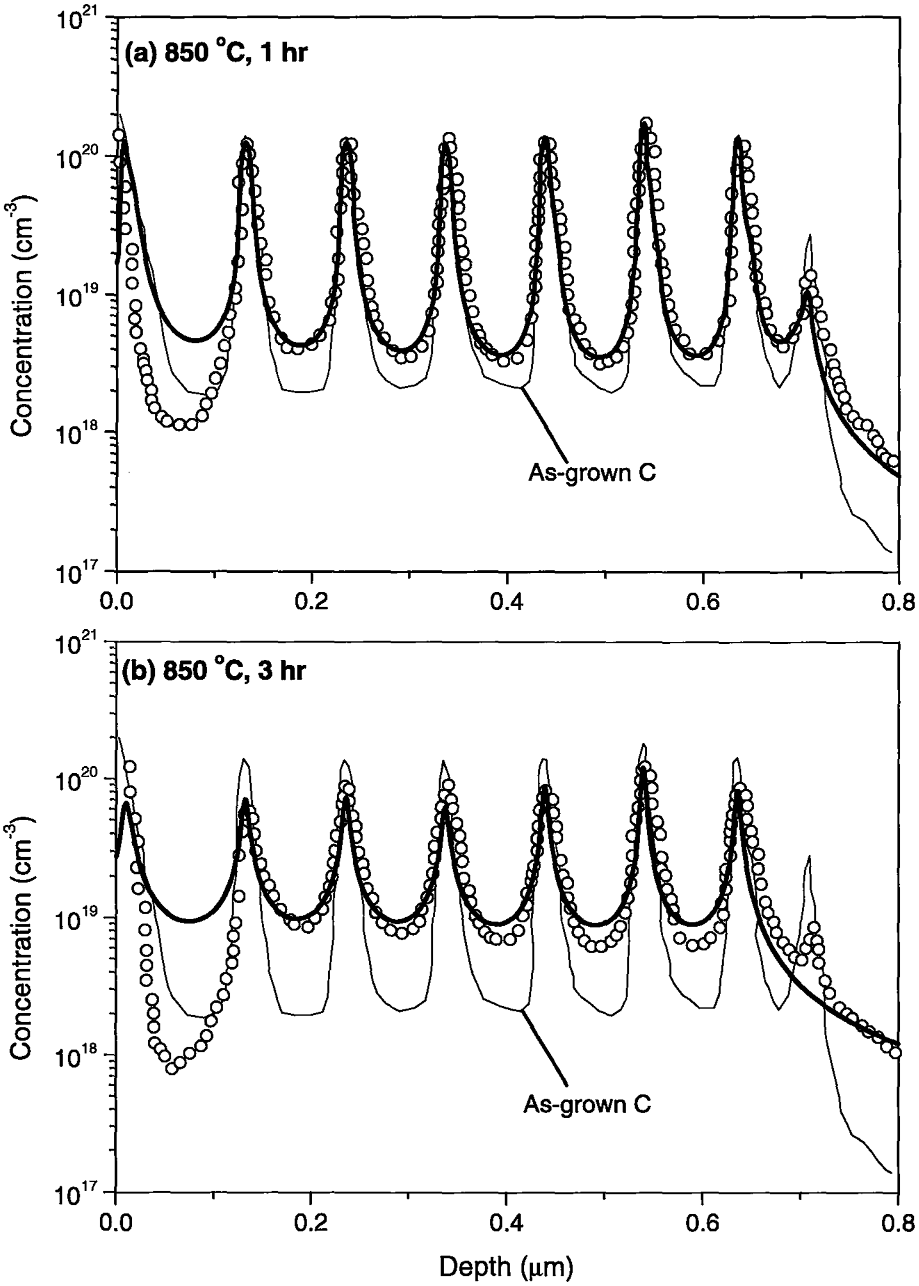

Figure 24: Experimental (symbols) and calculated (thick solid lines) carbon diffusion profiles for inert anneals at 850 °C for (a) 1 hr and (b) 3 hr. Data extracted from Ref. [48].

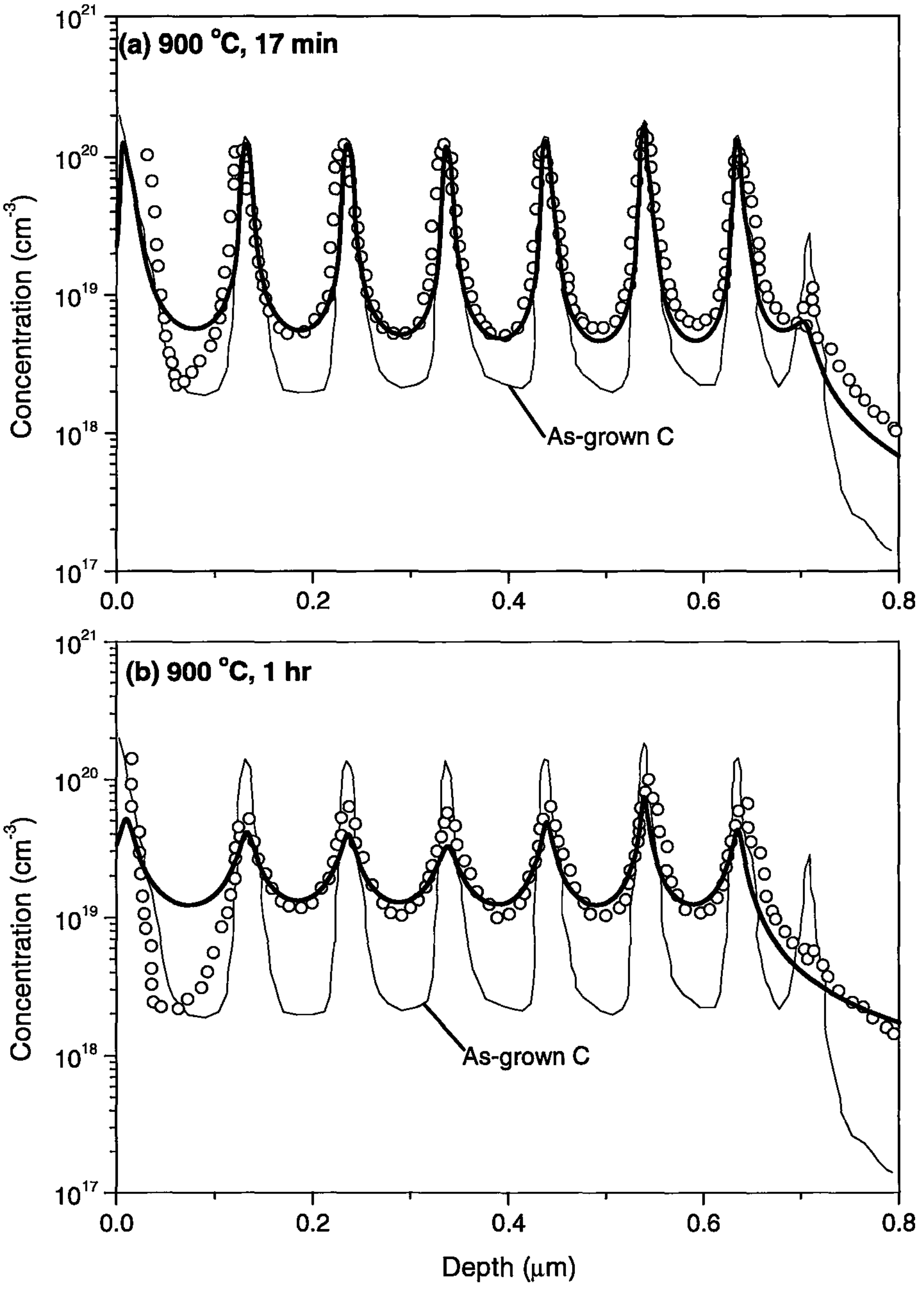

Figure 25: Experimental (symbols) and simulated (thick solid lines) carbon diffusion profiles for inert anneals at 900 °C for (a) 17 min and (b) 1 hr. Data extracted from Ref. [48].

5.3 Antimony Diffusion Enhancement by Carbon

The focus of this work is modeling C diffusion and its effect in suppressing B diffusion. However, in an attempt to verify our model for C diffusion, we extend this focus to include the effect of C in enhancing the diffusion of a vacancy mediated dopant. In this section, we use our model to verify the impact of C on the diffusion of antimony. This will be further elaborated in Chapter 6 in the section on the Frank-Turnbull reaction.

In the same study of Figure 18, Rucker *et al.* investigated the impact of C on dopants diffusing by a vacancy mechanism (arsenic and antimony) [46]. Similar to B, the As and Sb samples were prepared with uniform dopant concentration in the surface region, and then an epitaxial layer with and without C doping (10^{20} cm^{-3}). However, in contrast to B, which is an interstitial diffuser, As and Sb featured enhanced diffusion in the C doped samples after annealing at 900 °C in N_2. This was explained in terms of C outdiffusion via the Frank-Turnbull mechanism, which predicts that as C diffuses out of a C-rich region a supersaturation of vacancies is formed at that region.

The study has reported C profiles only for the B sample. We assumed the same as-grown C profile for the Sb sample as well, and used our model to verify the Sb diffusion experiment. Figure 26 shows very good agreement between the calculated and SIMS profiles after annealing for 6 hours for the samples with and without C doping.

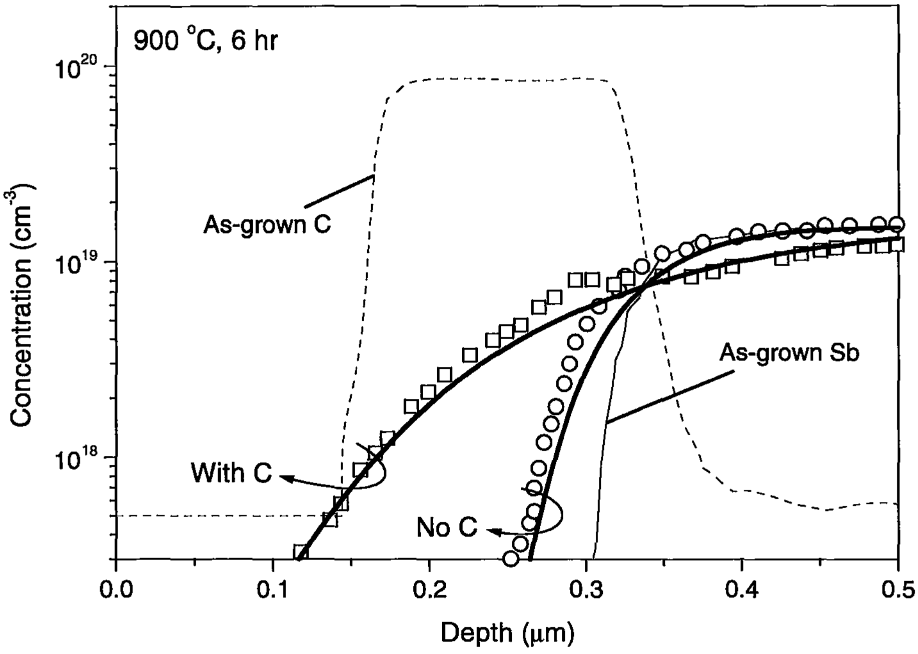

Figure 26: Diffusion of Sb from highly doped substrates in Si with and without C doping. Thick solid lines are the calculated profiles and symbols are SIMS data. Data extracted from Ref. [46].

5.4 The Carbon Clustering Reaction Reverse Rate

As previously mentioned, we determine the forward rate of the clustering reaction under diffusion limited conditions as $k_{f,\mathrm{Cl}} = 4\pi r D_{C_i}$, and vary the reverse rate ($k_{r,\mathrm{Cl}}$) as a fitting parameter, with the tendency of increased breakup of C_iC_s pairs at higher temperatures. The variation of $k_{r,\mathrm{Cl}}$ with temperature for the different simulated experiments is shown in Figure 27. We report, for the first time, an Arrhenius relation for $k_{r,\mathrm{Cl}}$, for which we obtain:

$$k_{r,\mathrm{Cl}} = 8\times10^{17} * \exp(-3.73\mathrm{eV}/kT)\,. \tag{34}$$

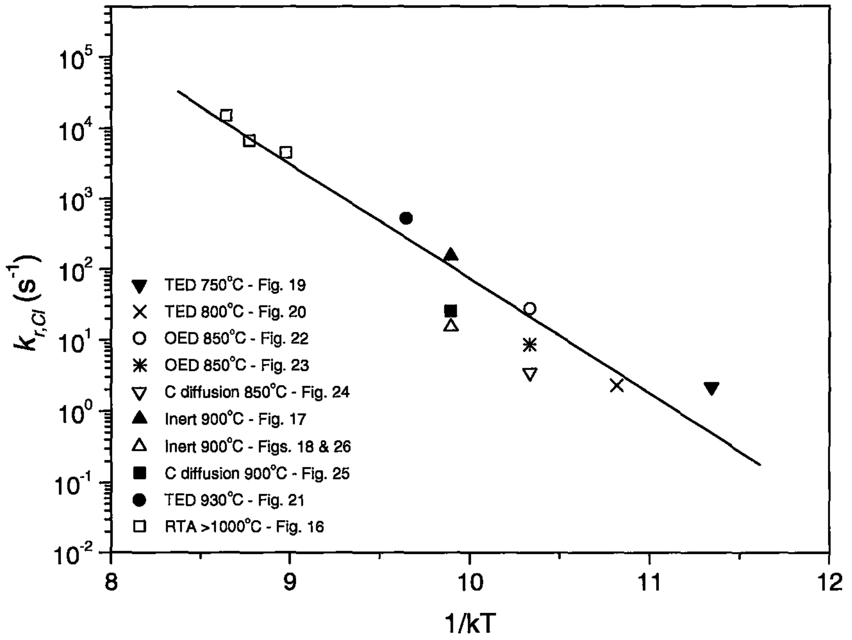

Figure 27: Variation of the reverse clustering rate with temperature for the simulated experiments.

Chapter 6

MODELING CARBON DIFFUSION WITHOUT THE CLUSTERING OR FRANK-TURNBULL MECHANISMS

In this chapter we explore simulations of the above samples without either the carbon clustering or the Frank-Turnbull reactions to verify the importance of these reactions for modeling C diffusion and its effect on B diffusion. Carbon acts as a trap for interstitials primarily through the kick-out mechanism, therefore it can't be excluded.

6.1 Excluding the Clustering Reaction

The carbon clustering reaction captures C_i atoms in immobile carbon complex pairs, thereby reducing the reverse kick-out reaction and the subsequent release of silicon interstitials. It is therefore generally expected that the exclusion of the clustering reaction would lead to: (1) enhanced C diffusion, where more C_i atoms are free to migrate, and (2) enhanced B diffusion.

We compared simulations for the samples studied in this work with and without the clustering effect. Using our model and set of parameters, we found that the removal of the clustering reaction had a more significant effect on the calculated profiles of low temperature samples compared to the higher temperature ones. For example, the calculated profiles in the samples of Figures 16 and 17 were not significantly affected by the removal of the clustering reaction, while they were considerably varied in the samples of Figures 18, 19(b), 20, 23(b), 24, and 25. Figure 28 shows the simulation results at 850 °C for the C diffusion sample of Figure 24(a), after excluding the clustering reaction. For this sample, it was necessary to reduce either D_I or C_I^* in the self-interstitial coefficient $D_I C_I^*$ by a factor of ~10 in order to overcome the observed discrepancy. Varying the C diffusion parameters, such as increasing $C_{C_s}^{\mathrm{eq}}$ by an order of ~2, was effective in reducing the C diffusion but not successful in obtaining a good match.

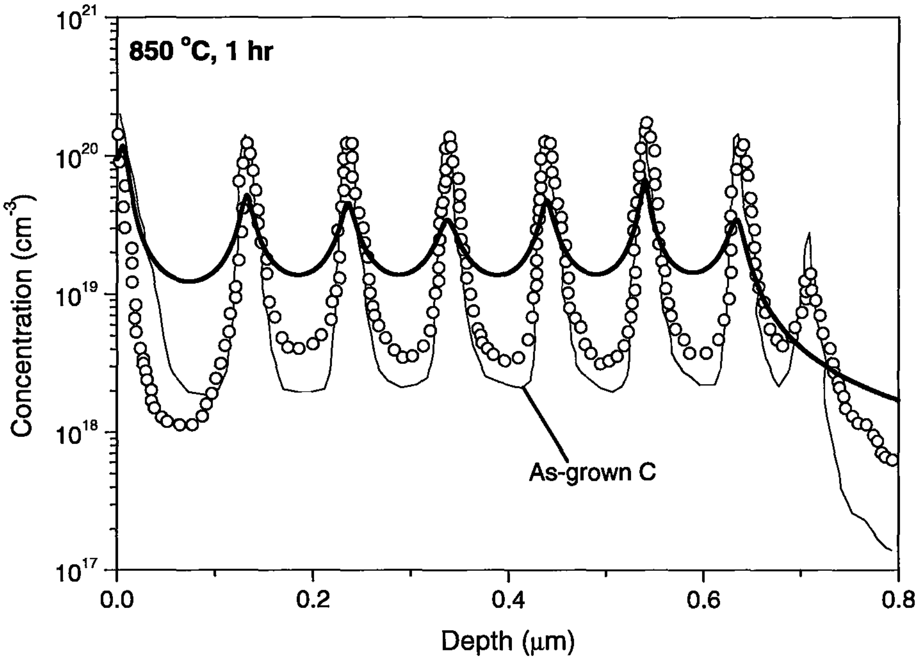

Figure 28: The effect of excluding the clustering reaction on the calculated profile (thick solid line) for C diffusion of a carbon doping superlattice after annealing in N_2. The annealed SIMS profile is plotted in symbols. Data extracted from Ref. [48].

In Figure 29 we also show the calculated B and C profiles without the clustering reaction for the sample of Figure 19(b), which underwent implantation and annealing at 750 °C. It can be seen that the removal of the clustering reaction affected the B and C profiles in the manner described above. Additionally, the BICs formation in the deeper boron marker layer is more evident compared to the results with the clustering mechanism. Reducing either D_I or C_I^*, as in the previous example, was successful in matching only the C profile. In order to match the B profile, we had to additionally reduce the B diffusivity which was originally calibrated according to the reference sample of the same study, as previously illustrated in Figure 19(a).

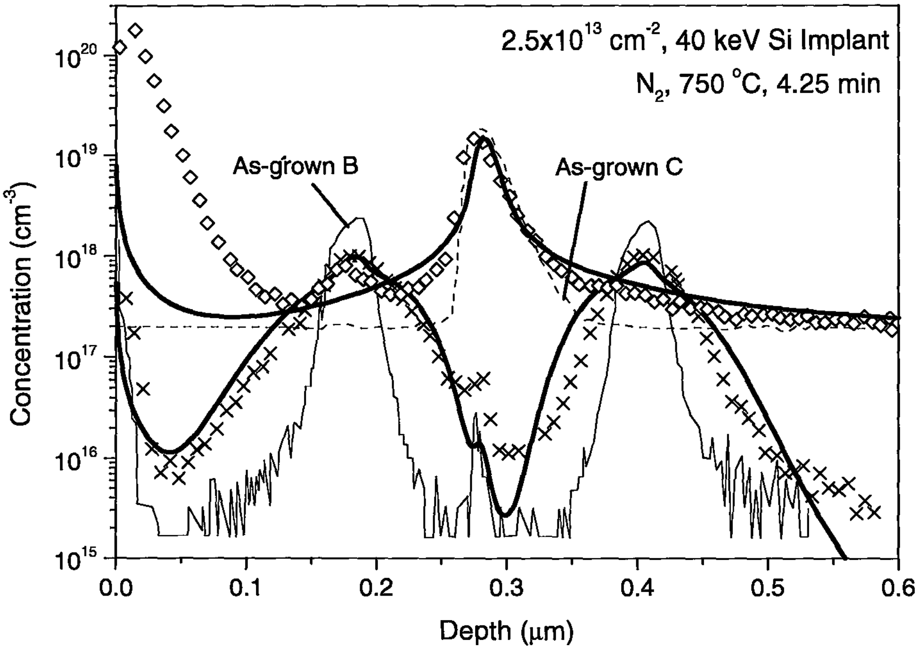

Figure 29: The effect of excluding the clustering reaction on the simulated profiles (thick solid lines) for B and C upon implantation and annealing. Symbols represent the SIMS data. Data extracted from Ref. [13].

The above leads us to conclude that it is not plausible to overcome the effect of removing the clustering reaction in the B and C profiles without considerably varying the involved diffusion parameters. Therefore, the clustering effect must be included in order to simulate a wide range of experimental structures, particularly low temperature samples, using the proposed literature parameters.

6.2 Excluding the Frank-Turnbull Reaction

The Frank-Turnbull mechanism assists C diffusion by forming C_i atoms, and creates a supersaturation of vacancies at C-rich regions due to C outdiffusion. However, under non-equilibrium conditions due to excess interstitials, the kick-out mechanism dominates and the Frank-Turnbull reaction plays a minor role [53].

We compared simulations for the B and C samples studied in this work with and without the Frank-Turnbull reaction. For diffusion under non-equilibrium conditions the calculated profiles for C and B diffusion were not significantly discrepant from the case with the FT reaction. However, for diffusion under equilibrium conditions insufficient C diffusion was observed, as expected. This can be seen in Figure 30 for one of the samples where the calculated profiles are obtained without the FT reaction. Additionally, in comparison with Figure 17 of the same sample, it can be noticed that a better match for the B profile was obtained with the FT reaction. Increasing either D_I or C_I^* in the self-interstitial coefficient $D_IC_I^*$ by a factor of 3, which is within the error bar of the literature data on $D_IC_I^*$ [54], was sufficient to obtain better correspondence for the C profiles. The suppression of a dopant diffusing primarily by interstitials due to C is attributed mainly to the depletion of interstitials. The presence of a vacancy supersaturation imposes a minor limitation for the contribution of vacancy assisted diffusion. Therefore, modeling C diffusion and its impact on B can be achieved without the Frank-Turnbull mechanism *per se*. However, in an attempt to simulate the antimony diffusion in the C doped sample, we were not able to predict any enhancement in the diffusion when the FT reaction was not accounted for. This leads us to conclude that a physics-based model for C diffusion must account for both the KO and FT reactions.

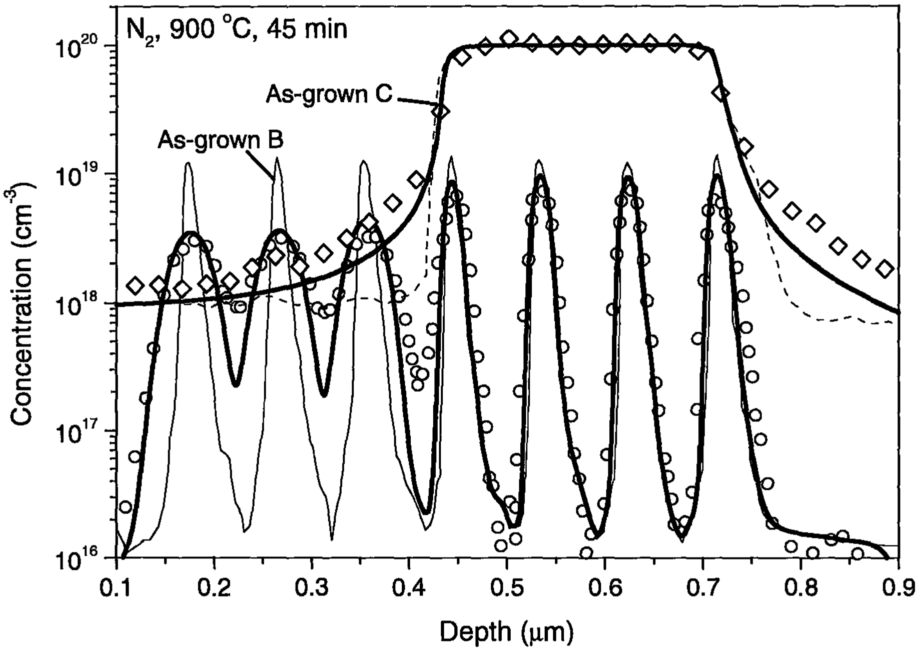

Figure 30: Simulations without the FT reaction (thick solid lines) for the diffusion of B spikes and C at 900 °C, 45 min in N_2. Symbols are SIMS data. Data extracted from Ref. [65].

Chapter 7

CONTRIBUTIONS AND FUTURE WORK

In this work we developed a consistent and complete model for carbon diffusion and its impact on boron diffusion in silicon and SiGe. In Chapter 2, the physical phenomena associated with boron and carbon diffusion were first reviewed. In Chapter 3, the previous efforts for modeling carbon diffusion were then presented. Despite the tremendous effort done in modeling carbon diffusion, we could not find a consistent model that describes the carbon diffusion behavior since most existing studies have focused on subsets of experimental data.

Chapter 4 presented a consistent and complete model for carbon diffusion and its impact on boron diffusion in silicon and SiGe. In Chapter 5, the model was verified over a wide range of structures for which data was available in the literature, and in Chapter 6 we showed the importance of all of the model reactions. The following sections summarize the contributions made in this work and present ideas for future work.

7.1 Contributions

This thesis introduces the first published consistent and complete model for the diffusion of carbon and its role in suppressing boron diffusion in silicon and silicon germanium. For carbon diffusion, we presented a physics-based model that describes reactions taking place on an atomic basis. These reactions are: (1) the kick-out reaction, (2) the Frank-Turnbull reaction, and (3) the carbon clustering reaction. When carbon outdiffusion takes place at C-rich areas, the kick-out reaction predicts the associated depletion of interstitials at those areas, while the Frank-Turnbull reaction predicts the associated vacancy supersaturation. The clustering reaction further reduces silicon interstitials. Using consistent well-established diffusion parameters, we showed that all of the above reactions must be accounted for to model carbon diffusion and its impact on dopant diffusion. Additionally, we reported, for the first time, Arrhenius relations for the forward and reverse rates of the clustering reaction. We assumed the forward rate of the clustering reaction under diffusion-limited conditions and used the reverse rate as a fitting parameter for which we obtained $k_{r,\mathrm{Cl}} = 8\times10^{17} * \exp(-3.73\mathrm{eV}/kT)$. To completely model boron diffusion in our work, we accounted for the boron interstitial clustering effect and the $\{311\}$ defects that are associated with boron TED.

To verify our model, we have successfully simulated a wide range of experimental structures. The test structures involved boron and/or carbon diffusion in Si and SiGe. The experimental conditions covered the complete temperature range of 750 - 1070 °C, and included diffusion in inert and oxidizing ambients, under RTA conditions, as well as in the presence of implant damage. Additionally, to verify the vacancy supersaturation that is associated with carbon outdiffusion, we simulated the impact of carbon on antimony diffusion.

7.2 Future Work

We have developed a consistent model for carbon diffusion in Si and SiGe. The model takes into account the kick-out and Frank-Turnbull mechanisms as well as the carbon clustering effect. Many carbon diffusion studies have considered the clustering phenomenon [45],[48],[49], while other studies have ignored it [12],[60],[64]. Additionally, several studies have considered only the initial step of the clustering process, whereas others have suggested additional complex clustering paths [48]. In two of the samples studied in this work that involved carbon diffusion at temperatures of 900 °C and above, we found that the implemented clustering reaction was not needed in order to fit the experimental results, while it was necessary for many lower temperature samples. However, maintaining the clustering reaction for both of the high temperature samples did not degrade the calculated matching profile. We are prevented by the lack of experiments from confirming that the clustering reaction can be excluded at high temperatures. Further experimental results would prove useful for this matter, which also entails a better insight into the kinetics of the carbon clustering phenomenon.

Using a $Si_{1-y}C_y/Si$ heterojunction system has been reported to confirm a band lineup that is more suitable for *pnp* HBT operation compared to $Si_{1-x}Ge_x/Si$, with phosphorus being the *n*-type base dopant [77]. Phosphorus is known to diffuse via an interstitial mechanism [78]. This opens the door for extending the study of this thesis to include the impact of carbon on phosphorus diffusion. This has not been sufficiently investigated compared to the boron case, and would therefore motivate ample research work.

REFERENCES

[1] G. E. Moore, Electronics **38** (1965).

[2] D. J. Paul, Semicond. Sci. Technol. **19**, R75 (2004).

[3] J. D. Cressler, IEEE Trans. Microwave Theory Tech. **46**, 572 (1998).

[4] J. D. Cressler and Guofu Niu, Silicon-Germanium Heterojunction Bipolar Transistors (Norwood, Massachusetts, 2003).

[5] U. König and A. Gruhle, in *1997 IEEE/Cornell Conference On Advanced Concepts in High Speed Semiconductor Devices and Circuits*, 4 – 6 Aug. 1997, pp. 14 – 23.

[6] G. Niu, J. D. Cressler, S. Zhang, A. Joseph, and D. Harame, in *2001 Topical Meeting on Silicon Monolithic Integrated Circuits in RF Systems*, Digest of Papers, 12 – 14 Sept. 2001, pp. 187 – 191.

[7] D. R. Greenberg, B. Jagannathan, S. Sweeney, G. Freeman, and D. Ahlgren, Tech. Dig. Int. Electron Devices Meeting **2002**, 787 (2002).

[8] A. Gruhle, IEEE Trans. Electron Devices **41**, 198 (1994).

[9] L. D. Lanzerotti, J. C. Sturm, E. Stach, R. Hull, T. Büyüklimanli, and C. Magee, Appl. Phys. Lett. **70**, 3125 (1997).

[10] E. J. Prinz, P. M. Garone, P. V. Schwartz, X. Xiao, and J. C. Sturm, IEEE Electron Device Lett., **12**, 42 (1991).

[11] P. A. Stolk, H.-J. Gossmann, D. J. Eaglesham, and J. M. Poate, Appl. Phys. Lett. **66**, 1370 (1995).

[12] A. Sibaja-Hernandez, M. W. Xu, S. Decoutere, and H. Maes, Mater. Sci. in Semi. Proc. **8**, 115 (2005).

[13] J. L. Ngau, P. B. Griffin, and J. D. Plummer, J. Appl. Phys. **90**, 1768 (2001).

[14] H. J. Osten, D. Endisch, E. Bugiel, B. Dietrich, G. G. Fischer, M. Kim, D. Krüger, and P. Zaumseil, Semicond. Sci. Technol. **11**, 1678 (1996).

[15] H. J. Osten, B. Heinemann, D. Knoll, G. Lippert, and H. Rücker, J. Vac. Sci. Technol. B **16**, 1750 (1998).

[16] A. Gruhle, H. Kibbel, and U. König, Appl. Phys. Lett. **75**, 1311 (1999).

[17] FLOOPS-ISE, version 9.0, from Synopsis, Inc., CA, USA.

[18] A. Sibaja-Hernandez, IMEC and Katholieke Universiteit Leuven, Belgium, Personal Communication, Mar. 2005.

[19] A. Benninghoven, F. G. Rüdenauer, and H. W. Werner, Secondary Ion Mass Spectrometry: Basic Concepts, Instrumental Aspects, Applications, and Trends, (Wiley, New York, 1987).

[20] http://presolar.wustl.edu/work/what_is_sims.html, accessed May 19, 2005.

[21] Y. M. Haddara and J. C. Bravman, Annu. Rev. Mater. Sci. **28**, 185 (1998).

[22] H. Bracht, in MRS Bulletin on Defects and Diffusion in Silicon Technology **25**, 22 (2000).

[23] F. C. Frank and D. Turnbull, Phys. Rev. **104**, 617 (1959).

[24] P. M. Fahey, P. B. Griffin, and J. D. Plummer, Rev. Mod. Phys. **61**, 289 (1989).

[25] V. C. Venezia, L. Pelaz, H.-J. L. Gossmann, A. Agarwal, and T. E. Haynes, Phys. Rev. B **69**, 125215 (2004).

[26] W. T. F. Fang. Ph. D. Thesis, *Modeling of Boron Diffusion in Silicon Germanium (With Implications for Modeling Dopant Diffusion in Silicon)*, Stanford University, 1996.

[27] A. F. W. Willoughby, J. M. Bonar, and A. D. N. Paine, Mat. Res. Soc. Symp. **568**, 253 (1999).

[28] N. E. B. Cowern, P. C. Zalm, P. van der Sluis, D. J. Gravesteijn, and W. B. de Boer, Phys. Rev. Lett. **72**, 2585 (1994).

[29] J. M. Bonar, B. M. McGregor, N. E. B. Cowern, A. Dan, G. A. Cooke, and A. F. W. Willoughby, Mat. Res. Soc. Symp. **610**, B4.9.1 (2000).

[30] P. Kuo, J. L. Hoyt, J. F. Gibbons, J. E. Tuner, and D. Lefforge, Appl. Phys. Lett. 67, 706 (1995).

[31] P. Kuo, J. L. Hoyt, J. F. Gibbons, J. E. Turner, and D. Lefforge, Appl. Phys. Lett. **66**, 580 (1995).

[32] N. Moriya, L. C. Feldman, H. S. Luftman, C. A. King, J. Bevk, and B. Freer, Phys. Rev. Lett. **71**, 883 (1993).

[33] F. K. LeGoues, R. Rosenberg, and B. S. Meyerson, Appl. Phys. Lett. **54**, 751 (1989).

[34] J. R. Pfiester and P. B. Griffin, Appl. Phys. Lett. **52**, 471 (1988).

[35] L. S. Robertson, M. E. Law, K. S. Jones, L. M. Rubin, J. Jackson, P. Chi, and D. S. Simons, Appl. Phys. Lett. 75, 3844 (1999)

[36] D. J. Eaglesham, P. A. Stolk, H.-J. Gossmann, and J. M. Poate, Appl. Phys. Lett. **65**, 2305 (1994).

[37] L. H. Zhang, K. S. Jones, P. H. Chi, and D. S. Simons, Appl. Phys. Lett. **67**, 2025 (1995).

[38] G. Mannino, N. E. B. Cowern, F. Roozeboom, and J. G. M. van Berkum, Appl. Phys. Lett. **76**, 855 (2000).

[39] P. A. Stolk, H.-J. Gossmann, D. J. Eaglesham, D. C. Jacobson, C. S. Rafferty, G. H. Gilmer, M. Jaraiz, J. M. Poate, H. S. Luftman, and T. E. Haynes, J. Appl. Phys. **81**, 6031 (1997).

[40] S. Solmi, M. Bersani, M. Sbetti, J. L. Hansen, and A. N. Larsen, J. Appl. Phys. **88**, 4547 (2000).

[41] C. S. Rafferty, G. H. Gilmer, M. Jaraiz, D. Eaglesham, and H.-J. Gossmann, Appl. Phys. Lett. **68**, 2395 (1996)

[42] M. E. Law and K. S. Jones, Tech. Dig. Int. Electron Devices Meeting **2000**, 511 (2000).

[43] S. Chakravarthi and S. T. Dunham, J. Appl. Phys. **89**, 3650 (2001).

[44] F. Rollert, N. A. Stolwijk, and H. Mehrer, Mater. Sci. Forum **38-41**, 753 (1989).

[45] S. Mirabella, A. Coati, D. De Salvador, E. Napolitani, A. Mattoni, G. Bisognim, M. Berti, A. Carnera, A. V. Drigo, S. Scalese, S. Pulvirenti, A. Terrasi, and F. Priolo, Phys. Review B **65**, 45209 (2002).

[46] H. Rücker, B. Heinemann, D. Bolze, D. Knoll, D. Krüger, R. Kurp, H. J. Osten, P. Schley, B. Tillack, and P. Zaumseil, Tech. Dig. Int. Electron Devices Meeting **1999**, 345 (1999).

[47] U. Gösele, A. Plößl and T. Y. Tan, in *Fourth International Symposium on Process Physics and Modeling in Semiconductor Devices*, edited by G.R. Srinivasan, C.S. Murthy, and S.T. Dunham (Electrochemical Society, Pennington, 1996), Electrochem. Soc. Proc. **96-4**, p. 309.

[48] R. Pinacho, P. Castrillo, M. Jaraiz, I. Martin-Bragado, J. Barbolla, H.-J. Gossmann, G.-H. Gilmer, and J.-L. Benton, J. Appl. Phys. **92**, 1582 (2002).

[49] P. A. Stolk, H.-J. Gossmann, D. J. Eaglesham, and J. M. Poate, Mater. Sci. Eng. **B36**, 275 (1996).

[50] M. S. Carroll. Ph. D. Thesis, *The Interaction of Silicon Self-interstitials and Substitutional Carbon in Silicon Based Heterostructures*, Princeton University, 2001.

[51] H. Rücker and B. Heinemann, Solid-State Electron. **44**, 783 (2000).

[52] K. Rajendran and W. Schoenmaker, Solid-State Electron. **45**, 229 (2001).

[53] H. Rücker, B. Heinemann, D. Bolze, R. Kurps, D. Krüger, G. Lippert, and H. J. Osten, Appl. Phys. Lett. **74**, 3377 (1999).

[54] H. Bracht, N. A. Stolwijk, and H. Mehrer, Phys. Rev. B **52**, 16542 (1995).

[55] A. Ural, P. B. Griffin, and J. D. Plummer, Phys. Rev. Lett. **83**, 3454 (1999).

[56] F. F. Morehead, Mater. Res. Soc. Symp. Proc. **104**, 99 (1988).

[57] T. Y. Tan and U. Gösele, Appl. Phys. A: Solids Surf. **37**, 1 (1985).

[58] H. Bracht, E. E. Haller, and R. Clark-Phelps, Phys. Rev. Lett. **81**, 393 (1998).

[59] P. Werner, H.-J. Gossmann, D. C. Jacobson, and U. Gösele, Appl. Phys. Lett. **73**, 2465 (1998).

[60] R. F. Scholz, P. Werner, U. Gösele and T. Y. Tan, Appl. Phys. Lett. **74**, 392 (1999).

[61] A. Pakfar, Mater. Sci. Eng. **B89**, 225 (2002).

[62] M. J. Aziz, Appl. Phys. Lett. **70**, 2810 (1997)

[63] Y. M. Haddara, B. T. Folmer, M. E. Law, and T. Büyüklimanli, Appl. Phys. Lett. **77**, 1976 (2000).

[64] R. Scholz, U. Gösele, J.-Y. Huh, and T. Y. Tan, Appl. Phys. Lett. **72**, 200 (1998).

[65] H. Rücker, B. Heinemann, W. Röpke, R. Kurps, D. Krüger, G. Lippert, and H. J. Osten, Appl. Phys. Lett. **73**, 1682 (1998).

[66] A. R. Bean and R. C. Newman, J. Phys. Chem. Solids **32**, 1211 (1971).

[67] A. K. Tipping and R. C. Newman, Semicond. Sci. Technol. **2**, 315 (1987).

[68] R. C. Newman and J. Wakefield, J. Phys. Chem. Solids **19**, 230 (1961).

[69] H. Rücker, B. Heinemann, W. Röpke, G. Fischer, G. Lippert, H. J. Osten, and R. Kurps, in *International Conference on Simulation of Semiconductor Processes and Devices* (IEEE, Piscataway, NJ, 1997), 8 – 10 Sept. 1998, pp. 281 - 284.

[70] L. Pelaz, M. Jaraiz, G. H. Gilmer, H.-J. Gossmann, C. S. Rafferty, D. J. Eaglesham, and J. M. Poate, Appl. Phys. Lett. **70**, 2285 (1997).

[71] S. Chakravarthi and S. T. Dunham, in *International Conference on Simulation of Semiconductor Processes and Devices, SISPAD* 1998, edited by K. D. Meyer (Springer-Verlag, Wien, Austria, 1998), 2 – 4 Sept. 1998, pp.55 - 58.

[72] N. E. B. Cowern, A. Cacciato, J. S. Cluster, F. W. Saris, and W. Vandervorst, Appl. Phys. Lett. **68**, 1150 (1996).

[73] H. G. Robinson. Ph. D. Thesis, *Diffusion of P-Type Dopants in Gallium Arsenide*, Stanford University, 1992.

[74] S. Rizk, Y. M. Haddara, A. Sibaja-Hernandez, in *Eighth International Workshop on Fabrication, Characterization, and Modeling of Ultra-Shallow Doping Profiles in Semiconductors, USJ-2005* (Daytona Beach, FL, USA, 2005), 5 – 8 Jun. 2005, pp. 315 – 322.

[75] M. S. Carroll and J. C. Sturm, Mat. Res. Soc. Symp. **610**, B4.10 (2000).

[76] M. S. Carroll, C-L. Chang, J. C. Sturm, and T. Büyüklimanli, Appl. Phys. Lett. 73, 3695 (1998).

[77] D. V. Singh, J. L. Hoyt, and J. F. Gibbons, Int. Electron Devices Meeting **2000**, 749 (2000).

[78] A. Ural, P. B. Griffin, and J. D. Plummer, J. Appl. Phys. **85**, 6440 (1999).